

# STEIN VARIATIONAL RARE EVENT SIMULATION \*

MAX EHRE<sup>†</sup>, IASON PAPAIOANNOU<sup>†</sup>, AND DANIEL STRAUB<sup>‡</sup>

**Abstract.** Rare event simulation and rare event probability estimation are important tasks within the analysis of systems subject to uncertainty and randomness. Simultaneously, accurately estimating rare event probabilities is an inherently difficult task that calls for dedicated tools and methods. One way to improve estimation efficiency on difficult rare event estimation problems is to leverage gradients of the computational model representing the system in consideration, e.g., to explore the rare event faster and more reliably. We present a novel approach for estimating rare event probabilities using such model gradients by drawing on a technique to generate samples from non-normalized posterior distributions in Bayesian inference – the Stein variational gradient descent. We propagate samples generated from a tractable input distribution towards a near-optimal rare event importance sampling distribution by exploiting a similarity of the latter with Bayesian posterior distributions. Sample propagation takes the shape of passing samples through a sequence of invertible transforms such that their densities can be tracked and used to construct an unbiased importance sampling estimate of the rare event probability – the Stein variational rare event estimator. We discuss settings and parametric choices of the algorithm and suggest a method for balancing convergence speed with stability by choosing the step width or base learning rate adaptively. We analyze the method’s performance on several analytical test functions and two engineering examples in low to high stochastic dimensions ( $d = 2 - 869$ ) and find that it consistently outperforms other state-of-the-art gradient-based rare event simulation methods.

**Key words.** Rare event simulation, Stein variational gradient descent, Sequential importance sampling,

**AMS subject classifications.** 62L99, 62P30, 62J02, 65C05

**1 Introduction and previous work** The goal of rare event simulation is to simulate outcomes of a model that belong to a predefined event whose occurrence probability is small (say,  $\leq 10^{-3}$ , your mileage may vary). Accurately estimating rare event and failure probabilities is relevant in a number of disciplines such as engineering design [25], structural reliability [33], chemical physics [1], finance [23], queueing theory [3], traffic management or systems biology [51]. In fields like engineering, finance or traffic management, the interest in such events is usually due to its associated severe adverse consequences, i.e., the event of interest is a failure event [51, 17, 33].

Technically, computing rare event probabilities requires integrating those tails of the model input parameter distribution that cover the rare event. Monte Carlo integration is inefficient for evaluating such tail integrals as, at a fixed estimation accuracy, the required number of samples scales inversely with the rare event probability. Early approaches to efficiently approximate rare event probabilities were based on first- and second-order Taylor expansions of the hypersurface separating the rare event from the remaining input parameter space [49, 9, 16]. The probability content of the resulting approximations can be computed with ease but these approaches are limited to relatively low parameter dimensions [56] and problems with a single convex failure domain. Advanced sampling-based methods aim at reducing the number of required samples at constant estimation error compared to Monte Carlo. Proponents of such methods are classic variance reduction techniques like importance sampling [10, 24, 4] and its sequential variants [7, 47], in which importance sampling is applied repeatedly to sample from a sequence of distributions that converges towards an optimal (zero-variance) importance sampling density of the rare event. Markov chain Monte Carlo (MCMC) schemes are used to propagate samples between subsequent distributions in the sequence [11, 47]. These approaches are essentially sequential Monte Carlo (SMC) methods [18, 41] that have been repurposed for exploring rare events rather than Bayesian posterior distributions. A popular variant of rare event-oriented SMC known as multilevel splitting [26, 52] or subset simulation [5] is based on a particular (discontinuous) choice of intermediate distribution. The performance of subset simulation is largely determined by the efficiency and robustness of the chosen MCMC algorithm [46]. If gradient information of the model is available, using gradient-based MCMC samplers such as Hamiltonian Monte Carlo (HMC) [19, 42] may improve the performance of subset simulation [61]. [48] proposed to use HMC for directly sampling from a near-optimal rare event importance sampling density.

\*Submitted to the editors DATE.

**Funding:** This project was supported by the German Research Foundation (DFG) through Grant STR 1140/6-1 under SPP 1886.

<sup>†</sup>Engineering Risk Analysis Group, Technical University of Munich (max.ehre@tum.de,iason.papaioannou@tum.de,straub@tum.de). ■

Stein variational gradient descent (SVGD) is an algorithm for sampling from Bayesian posteriors without knowing the model evidence or – more generally – for sampling from non-normalized target distributions without knowing the normalization constant [38]. The principal idea is to pass a set of samples initially drawn from a tractable reference distribution through a sequence of invertible transforms that are chosen from a reproducing kernel Hilbert space such that the samples converge towards the target distribution. SVGD has grown to be a viable alternative to MCMC and has been successfully applied in various tasks connected to sampling from Bayesian posteriors such as uncertainty quantification in stochastic PDEs [65], deep learning [59] and training diversified mixture models [60]. Theoretical analyses of SVGD are available in [36, 34, 40, 32, 44]. Several relevant improvements have been made to SVGD such as using surrogate models of the target to drive a gradient-free version of SVGD [30] and subspace SVGD methods [12, 39] that aim at resolving a variance degeneracy issue faced when using SVGD in high parameter dimensions [6].

In this contribution, we introduce the Stein variational rare event (SVRE) estimator. The SVRE estimator is an importance sampling estimator that relies on repurposing SVGD for sampling near-optimal, smoothed rare event importance densities. Following [29], we obtain an unbiased rare event probability estimate using the final generation of SVRE-generated samples. We suggest an alternative approach for building the target probability estimate based on a sample drawn from a Gaussian mixture sample that is trained on the final SVRE sample generation. We also discuss an approximation that allows choosing the base learning rate adaptively such as to strike a good balance between accuracy and convergence speed. The manuscript is organized as follows: [Section 2](#) introduces the rare event estimation problem and briefly covers importance sampling estimates of rare event probabilities in [Subsection 2.1](#). In the remainder of [Section 2](#), we give a review of the principles underlying SVGD and the original SVGD algorithm. [Section 3](#) lays out our method for estimating rare event probabilities with the SVRE estimator. [Section 4](#) provides empirical results on a number of test functions and engineering examples and conclusions are given in [Section 5](#).

## 2 Background & Theory

**2.1 Rare event estimation** Let  $\mathbf{X}$  be a  $d$ -dimensional random vector that is absolutely continuous with respect to Lebesgue measure and has joint probability density function (PDF)  $p_0(\mathbf{x})$ . Let  $\mathcal{X}$  denote the outcome space  $\mathbf{X}$  maps to so that each realization of the random vector  $\mathbf{x} \in \mathcal{X}$ . We define a rare event as  $\mathcal{F} = \{\mathbf{x} : g(\mathbf{x}) \leq 0\}$ , where  $g(\mathbf{x})$  is a performance function that indicates whether a given state  $\mathbf{x}$  belongs to the rare event. In reliability analysis, the rare event corresponds to a failure event and the performance function is known as limit state function (LSF). The probability of the failure event is

$$(2.1) \quad p_{\mathcal{F}} = \int_{\mathcal{F}} p(\mathbf{x}) d\mathbf{x} = \int_{\mathcal{X}} \mathbb{I}[g(\mathbf{x}) \leq 0] p_0(\mathbf{x}) d\mathbf{x} = \mathbb{E}_{p_0} [\mathbb{I}(g(\mathbf{X}) \leq 0)],$$

where the indicator function  $\mathbb{I}[\cdot]$  equals 1 if the condition in the argument is true and 0 otherwise. The Monte Carlo estimator of (2.1) using  $n$  independent samples from  $p_0(\mathbf{x})$  has coefficient of variation  $\sqrt{(1 - p_{\mathcal{F}})/(np_{\mathcal{F}})}$ , which becomes large for small  $p_{\mathcal{F}}$ , i.e., for rare event probabilities. Importance sampling (IS) belongs to a class of methods known as variance reduction techniques and can improve the situation significantly by sampling from a density  $h$  rather than  $p_0$ , where  $h$  should cover the failure event better than  $p_0$ . Let  $h$  be a PDF such that  $h(\mathbf{x}) > 0$  whenever  $g(\mathbf{x}) \leq 0$ . Then, one can rewrite (2.1) as

$$(2.2) \quad p_{\mathcal{F}} = \int_{\mathcal{X}} \mathbb{I}[g(\mathbf{x}) \leq 0] \overbrace{\frac{p_0(\mathbf{x})}{h(\mathbf{x})}}{:=\omega(\mathbf{x})} h(\mathbf{x}) d\mathbf{x} = \mathbb{E}_h [\mathbb{I}(g(\mathbf{X}) \leq 0) \omega(\mathbf{X})],$$

which leads to the (unbiased) IS estimator

$$(2.3) \quad \hat{p}_{\mathcal{F}} = \frac{1}{n} \sum_{k=1}^n \mathbb{I}[g(\mathbf{x}_k) \leq 0] \omega(\mathbf{x}_k), \quad \mathbf{x}_k \sim h.$$

The efficiency of IS depends on the choice of  $h$ , the selection of which is nontrivial and an ongoing research topic [47, 62, 13, 54]. An optimal importance density  $h^*$  in the sense that the associated estimator's coefficient of variation is zero, reads

$$(2.4) \quad h^*(\mathbf{x}) = \frac{\mathbb{I}[g(\mathbf{x}) \leq 0] p_0(\mathbf{x})}{p_{\mathcal{F}}}.$$

The normalizing constant of  $h^*$  is  $p_{\mathcal{F}}$  – the sought rare event probability. Hence, sampling from  $h^*$  requires sampling from a PDF without knowing its normalizing constant.

**2.2 Variational inference with reversible transformations** Variational inference (VI) refers to a class of methods motivated by Bayesian inference that facilitate sampling from non-normalized posterior distributions via optimization. The basic idea is to approximate the non-normalized posterior  $\tilde{p} = p(\mathbf{x})Z$  with  $Z = \int \tilde{p}(\mathbf{x})d\mathbf{x}$  using another distribution  $q \in \mathcal{Q}$  [8].  $\mathcal{Q}$  is often chosen as a parametrized family of distributions. The goal is to find a  $q$  that is most similar to  $p$  in some sense. Usually, the Kullback-Leibler-divergence is used as a discrepancy measure such that the VI problem reads

$$(2.5) \quad q^*(\mathbf{x}) = \arg \min_{q \in \mathcal{Q}} D_{\text{KL}}(q||p) = \arg \min_{q \in \mathcal{Q}} \mathbb{E}_q[\log q] - \mathbb{E}_q[\log \tilde{p}] + \log Z.$$

$\log Z$  is independent of  $q$  and hence can be neglected for solving the optimization problem. A key challenge in any VI method is the choice of  $\mathcal{Q}$ , which should be simple enough to keep the optimization problem tractable but sufficiently expressive to allow for approximating complex posterior distributions. Parametric distribution families often fail to accomplish the latter. In SVGD,  $\mathcal{Q}$  is defined implicitly as the set of distributions obtained by pushing a random vector  $\mathbf{X} \sim q_0$  through a sequence of  $T$  bijective transforms  $\{\mathcal{T}_t : \mathcal{X} \rightarrow \mathcal{X}\}_{t=1}^T$  [38]. For any bijective transform  $\mathcal{T}$ , we call the distribution of  $\mathbf{Z} = \mathcal{T}(\mathbf{X})$  with  $\mathbf{X} \sim q_0$  the pushforward of  $q_0$  under  $\mathcal{T}$  and denote it as  $\mathcal{T}_{\#}q_0$ . Further, we denote the pushforward of  $q_0$  under  $\mathcal{T}_t \circ \dots \circ \mathcal{T}_1$  as  $q_t := (\mathcal{T}_t \circ \dots \circ \mathcal{T}_1)_{\#}q_0$  ( $t = 1, \dots, T$ ). In SVGD,  $\mathcal{Q} = \{(\mathcal{T}_t)_{\#}q_0 : (\mathcal{T}_t \circ \dots \circ \mathcal{T}_1)_{\#}q_0\}$ , where the  $\{\mathcal{T}_t\}_{t=1}^T$  are chosen as

$$(2.6) \quad \mathcal{T}_t(\mathbf{x}) = \mathbf{x} + \epsilon \phi_t(\mathbf{x}) \quad (t = 1, \dots, T).$$

$\phi_t : \mathcal{X} \rightarrow \mathcal{X}$  is a smooth, bounded vector-valued function and  $\epsilon$  is a learning rate.  $\phi_t$  can be interpreted as a velocity field along which particles living in  $\mathcal{X}$  flow for a time  $\epsilon$ . Choosing  $\epsilon < 1$  ensures that  $\mathcal{T}_t(\mathbf{x})$  is close to the identity map and bijective such that by the transformation of variables theorem

$$(2.7) \quad q_T(\mathbf{x}) = q_0(\mathbf{x}) \prod_{t=1}^T |\det \nabla \mathcal{T}_t(\mathbf{x})|^{-1}.$$

Starting from  $q_0$ , the main task in SVGD is to find a sequence of velocity fields that minimize  $D_{\text{KL}}(q_t||p)$  in each step  $t = 1, \dots, T$ . This corresponds to solving the following optimization problem in each step [38]:

$$(2.8) \quad \begin{aligned} \phi_t(\mathbf{x}) &= - \arg \min_{\phi \in \mathcal{P}} \nabla_{\epsilon} D_{\text{KL}}(q_t||p) \Big|_{\epsilon=0} \\ &= - \arg \min_{\phi \in \mathcal{P}} \nabla_{\epsilon} D_{\text{KL}}(q_{t-1}||\mathcal{T}_t^{-1}p) \Big|_{\epsilon=0} \\ &= \arg \max_{\phi \in \mathcal{P}} \mathbb{E}_{q_{t-1}} [\nabla_{\epsilon} \log \mathcal{T}_t^{-1}p] \Big|_{\epsilon=0} \\ &= \arg \max_{\phi \in \mathcal{P}} \mathbb{E}_{q_{t-1}} [\nabla_{\mathbf{x}} \log p(\mathcal{T}_t(\mathbf{x}))^{\text{T}} \phi_t(\mathbf{x}) + \text{trace}((\mathbf{I} + \epsilon \nabla_{\mathbf{x}} \phi_t(\mathbf{x}))^{-1} \cdot \nabla_{\mathbf{x}} \phi_t(\mathbf{x}))] \Big|_{\epsilon=0} \\ &= \arg \max_{\phi \in \mathcal{P}} \mathbb{E}_{q_{t-1}} [\text{trace}(\mathcal{A}_p \phi_t(\mathbf{x}))], \end{aligned}$$

where  $\mathcal{A}_p \phi_t(\mathbf{x}) = \nabla_{\mathbf{x}} \log p(\mathbf{x})^{\text{T}} \phi_t(\mathbf{x}) + \nabla_{\mathbf{x}} \phi_t(\mathbf{x})$  is a so-called Stein operator. Next, we introduce kernels and reproducing kernel Hilbert spaces (RKHS) and outline the role these objects play in the context of SVGD.

**2.3 Kernels and RKHS** Let  $k : \mathcal{X} \times \mathcal{X} \rightarrow \mathbb{R}$  be a symmetric, positive definite function. The closure of  $\{f : f(\mathbf{x}) = \sum_{i=1}^{\infty} a_i k(\mathbf{x}, \mathbf{y}_i)\}$  is the unique reproducing kernel Hilbert space of  $k$ ,  $\mathcal{H}$  [2]. Since  $k$  is positive definite,  $\mathcal{H}$  can be equipped with the inner product  $\langle f, g \rangle_{\mathcal{H}} = \sum_{i=1}^{\infty} \sum_{j=1}^{\infty} a_i b_j k(\mathbf{x}_j, \mathbf{y}_i)$  with  $g(\mathbf{y}) = \sum_{j=1}^{\infty} b_j k(\mathbf{x}_j, \mathbf{y}) \in \mathcal{H}$  and norm  $\|f\|_{\mathcal{H}}^2 = \langle f, f \rangle_{\mathcal{H}}$ . Further, let  $\mathcal{H}^d = \times_{i=1}^d \mathcal{H}$  be a product Hilbert space of  $d \times 1$ -vector-valued functions  $\mathbf{f} = [f_1, \dots, f_d]^{\text{T}}$  with  $\{f_i \in \mathcal{H}\}_{i=1}^d$  and inner product  $\langle \mathbf{f}, \mathbf{g} \rangle_{\mathcal{H}^d} = \sum_{i=1}^d \langle f_i, g_i \rangle_{\mathcal{H}}$ , where  $\mathbf{g} = [g_1, \dots, g_d]^{\text{T}} \in \mathcal{H}^d$ . The norm in  $\mathcal{H}^d$  is defined as  $\|\mathbf{f}\|_{\mathcal{H}^d}^2 = \sum_{i=1}^d \langle f_i, f_i \rangle_{\mathcal{H}} = \sum_{i=1}^d \|f_i\|_{\mathcal{H}}^2$ .  $k$  can be always expressed in terms of a (non-unique) map  $\phi : \mathcal{X} \rightarrow \mathcal{H}^d$  (known as the feature map) as  $k(\mathbf{x}, \mathbf{y}) = \langle \phi(\mathbf{x}), \phi(\mathbf{y}) \rangle_{\mathcal{H}^d}$ . The two key properties of the RKHS  $\mathcal{H}^d$  are [53] are:

1.  $k(\mathbf{x}, \cdot) \in \mathcal{H}^d$ .
2.  $f(\mathbf{x}) = \langle f(\cdot), k(\mathbf{x}, \cdot) \rangle_{\mathcal{H}^d}$ .

The first property states that the canonical map  $k(\mathbf{x}, \cdot)$  is in the RKHS and is implied in the definition of the inner product of the RKHS. The second property is the reproducing property and states that the evaluation operator of any function in the RKHS at  $\mathbf{x}$  can be expressed as an inner product of said function with the canonical map evaluated at  $\mathbf{x}$ . Effectively, this is a smoothness constraint on the elements of the RKHS and the key to obtain a closed-form solution of (2.8) once the search space is chosen as  $\mathcal{H}$ .

**2.4 Stein discrepancy and optimal KL descent** Let  $q$  and  $p$  be PDFs of distributions supported on  $\mathcal{X}$  and assume  $\phi(\mathbf{x})$  satisfies

$$\int_{\mathcal{X}} \nabla_{\mathbf{x}}(p(\mathbf{x})\phi^{\top}(\mathbf{x}))d\mathbf{x} = \mathbf{0}.$$

Then,  $\phi$  is said to be in the Stein class of  $p$  and

$$(2.9) \quad \mathbb{E}_q[\mathcal{A}_p\phi(\mathbf{x})] = \mathbf{0} \text{ iff } q = p \text{ with } \mathcal{A}_p\phi_t(\mathbf{x}) = \nabla_{\mathbf{x}} \log p(\mathbf{x})^{\top}\phi_t(\mathbf{x}) + \nabla_{\mathbf{x}}\phi_t(\mathbf{x})$$

as defined below (2.8). For  $q = p$ , (2.9) is known as Stein's identity and maximizing the violation of Stein's identity over  $\mathcal{P}$  if  $q \neq p$  gives rise to a statistical divergence measure known as Stein discrepancy  $\mathbb{D}(p, q)$ , which expresses how different  $q$  and  $p$  are [27]:

$$(2.10) \quad \mathbb{D}(p, q) := \max_{\phi \in \mathcal{P}} \mathbb{E}_q[\text{trace}(\mathcal{A}_p\phi(\mathbf{x}))].$$

The choice of  $\mathcal{P}$  – known as the Stein set – plays a similar role as the choice of  $\mathcal{Q}$  in VI: very general choices of  $\mathcal{F}$  (e.g., all Lipschitz-differentiable functions) render the above maximization intractable whereas too specific choices of  $\mathcal{F}$  may overly constrain the search space and lead to  $\mathbb{D}(p, q) = 0$  even if  $q \neq p$  [37].

Constraining  $\mathcal{P}$  to a unit ball in  $\mathcal{H}^d$  and assuming  $k$  is in the Stein class of  $p$ , one may use the reproducing property – namely  $f(\mathbf{x}) = \langle f(\cdot), k(\mathbf{x}, \cdot) \rangle_{\mathcal{H}^d}$  and  $\nabla_{\mathbf{x}}f(\mathbf{x}) = \langle f(\cdot), \nabla_{\mathbf{x}}k(\mathbf{x}, \cdot) \rangle_{\mathcal{H}^d}$  – to obtain a *kernelized Stein discrepancy* [14, 37]

$$(2.11) \quad \mathbb{S}(p, q) = \max_{\substack{\phi \in \mathcal{H}^d \\ \|\phi\|_{\mathcal{H}^d} \leq 1}} \mathbb{E}_q[\text{trace}(\mathcal{A}_p\phi(\mathbf{x}))] = \max_{\substack{\phi \in \mathcal{H}^d \\ \|\phi\|_{\mathcal{H}^d} \leq 1}} \langle \phi(\cdot), \mathcal{A}_pk(\mathbf{x}, \cdot) \rangle_{\mathcal{H}^d}$$

Following from the right-hand side in (2.11), we can compute  $\mathbb{S}(p, q)$  by choosing  $\phi \propto \mathcal{A}_pk(\mathbf{x}, \cdot)$  and normalizing such that

$$(2.12) \quad \mathbb{S}(p, q_{t-1}) = \mathbb{E}_{q_{t-1}} \left[ \text{trace} \left( \mathcal{A}_p \frac{\phi_t^*(\mathbf{x})}{\|\phi_t^*(\mathbf{x})\|_{\mathcal{H}^d}} \right) \right] \text{ with } \phi_t^*(\cdot) = \mathbb{E}_{q_{t-1}}[\nabla_{\mathbf{x}} \log p(\mathbf{x})^{\top}k(\mathbf{x}, \cdot) + \nabla_{\mathbf{x}}k(\mathbf{x}, \cdot)]$$

This implies that

$$(2.13) \quad \mathbb{S}(p, q_{t-1}) = \sqrt{\mathbb{E}_{q_{t-1}}[\text{trace}(\mathcal{A}_p^{\mathbf{x}}\mathcal{A}_p^{\mathbf{y}}k(\mathbf{x}, \mathbf{y}))]} = \langle \phi_t^*, \mathcal{A}_pk(\mathbf{x}, \cdot) \rangle_{\mathcal{H}^d} = \|\phi_t^*\|_{\mathcal{H}^d},$$

where  $\mathcal{A}_p^{\mathbf{x}}$  acts on the first argument of  $k$  and  $\mathcal{A}_p^{\mathbf{y}}$  acts on the second argument of  $k$ . Comparing (2.10) and (2.8) reveals that transporting  $\mathbf{x} \sim q_{t-1}$  along  $\phi_t^*$  for a step width  $\epsilon_t$  reduces the KL divergence with the target  $p$  by an amount  $\mathbb{S}(p, q_{t-1})$ .

This facilitates an iterative procedure that successively drives the sequence of variational distributions  $\{q_t\}_{t=1}^T$  closer to  $p$ . The expectation  $\mathbb{E}_{q_{t-1}}[\cdot]$  in (2.12) is approximated with a finite number of samples/particles that are initially drawn from the first (tractable) variational PDF  $q_0$  and subsequently propagated. The original SVGD algorithm is outlined in Algorithm 1.

**Algorithm 1:** SVGD [38]

---

**Input** : target PDF  $p(\mathbf{x})$ , kernel  $k(\mathbf{x}, \mathbf{x}')$ ,  $n$  prior samples  $\{\mathbf{x}_i^0\}_{i=1}^n \sim p_0$   
**Output**:  $n$  posterior samples  $\{\mathbf{x}_i \sim p\}$   
**for**  $t = 0, \dots, T$  **do**  
     $\mathbf{x}_i^{t+1} = \mathbf{x}_i^t + \epsilon_t \widehat{\phi}_t^*(\mathbf{x}_i^t)$  with  $\widehat{\phi}_t^*(\mathbf{y}) = \frac{1}{n} \sum_{i=1}^n k(\mathbf{x}_i^t, \mathbf{y}) \nabla_{\mathbf{x}} \log p(\mathbf{x}_i^t) + \nabla_{\mathbf{x}} k(\mathbf{x}_i^t, \mathbf{y})$   
**end**

---

**3 SVRE: Stein variational rare event estimation**

**3.1 Method** In this section we formulate our method that aims at repurposing the original SVGD to simulate samples from a given rare event  $\mathcal{F}$  and subsequently estimating the associated rare event probability with importance sampling based on the final generation of samples. To this end we exploit a similarity between a generic Bayesian posterior distribution

$$(3.1) \quad p_{\text{post}}(\mathbf{x}) = \frac{L(\mathbf{x})p_{\text{prior}}(\mathbf{x})}{Z}$$

and the optimal rare event importance sampling density in (2.4). In particular, the posterior  $p_{\text{post}}(\mathbf{x})$  and the optimal rare IS density  $h^*(\mathbf{x})$  are both products of two pointwise known functions and an unknown normalization constant. Therein, the likelihood  $L(\mathbf{x})$  corresponds to the indicator  $\mathbb{I}[g(\mathbf{x}) \leq 0]$ , the prior  $p_{\text{prior}}(\mathbf{x})$  corresponds to the nominal PDF  $p_0(\mathbf{x})$  and the evidence  $Z$  corresponds to the rare event probability  $p_{\mathcal{F}}$ . This analogy has been leveraged to repurpose Bayesian inference approaches for sampling from rare event optimal IS densities in [47, 54, 58, 21].

In practice, it is necessary to smoothen the rare event indicator function  $\mathbb{I}[g(\mathbf{x}) \leq 0]$ . Here, we use the logistic CDF to obtain a smoothened indicator of the form

$$(3.2) \quad F(\mathbf{x}) = \frac{1}{2} \left( 1 + \tanh \left( -\frac{\pi}{\sqrt{3}} \frac{\mu + g(\mathbf{x})}{2\sigma} \right) \right) \quad \text{with} \quad \nabla_{\mathbf{x}} \log F(\mathbf{x}) = -\frac{\pi \nabla_{\mathbf{x}} g(\mathbf{x})}{2\sqrt{3}\sigma} \left( 1 - \tanh \left( -\frac{\pi}{\sqrt{3}} \frac{\mu + g(\mathbf{x})}{2\sigma} \right) \right).$$

$\mu$  is the mean of the logistic RV and controls the location of the smooth indicator. The choice  $\mu = -\sqrt{3}\sigma/\pi \log(P/(1-P))$  places probability mass  $P$  in the failure domain, where we select  $P = 0.9$ .  $\sigma$  is the standard deviation of the logistic RV and acts as a smoothing parameter. Fig. 1 depicts the smoothened indicator for different choices of  $\mu$  and  $\sigma$  and shows that the choice of  $\mu$  is of negligible relevance when  $\sigma \leq 0.01$ . Plugging (3.2) for the indicator in (2.4), we obtain a smooth rare event IS density that can be defined as a target PDF:

$$(3.3) \quad p(\mathbf{x}) := \frac{F(\mathbf{x})p_0(\mathbf{x})}{\tilde{p}_{\mathcal{F}}} \quad \text{with} \quad \tilde{p}_{\mathcal{F}} = \int_{\mathcal{X}} F(\mathbf{x})p_0(\mathbf{x})d\mathbf{x}.$$

Consequently, the optimal map in step  $t$  reads

$$(3.4) \quad \phi_t^*(\cdot) = \mathbb{E}_{q_{t-1}}[(\nabla_{\mathbf{x}} \log F(\mathbf{x}) + \nabla_{\mathbf{x}} \log p_0(\mathbf{x}))^T k(\mathbf{x}, \cdot) + \nabla_{\mathbf{x}} k(\mathbf{x}, \cdot)].$$

Upon running SVGD for  $T$  iterations in order to simulate  $n$  samples from  $p(\mathbf{x})$ , the obtained samples  $\{\mathbf{x}_i^T\}_{i=1}^n$  follow the final variational IS distribution  $q_T$ . The importance sampling estimate of the rare event probability reads

$$(3.5) \quad \hat{p}_{\mathcal{F}}^{\text{SVRE}} = \frac{1}{n} \sum_{i=1}^n \mathbb{I}[g(\mathbf{x}_i^T) \leq 0] \frac{p_0(\mathbf{x}_i^T)}{q_T(\mathbf{x}_i^T)} \quad \text{with} \quad \mathbf{x}_i^T \sim q_T,$$

where  $q_T$  is evaluated by tracking the Jacobians of all the  $\{\mathcal{T}_t\}_{t=1}^T$  using (2.7). An estimate of the coefficient of variation of  $\hat{p}_{\mathcal{F}}^{\text{SVRE}}$  is given as

$$(3.6) \quad \widehat{\delta}_{\mathcal{F}}^{\text{SVRE}} = \sqrt{\frac{\sum_{i=1}^n w_i^2}{(\sum_{i=1}^n w_i)^2} - \frac{1}{n}} \quad \text{where} \quad w_i := \mathbb{I}[g(\mathbf{x}_i^T) \leq 0] \frac{p_0(\mathbf{x}_i^T)}{q_T(\mathbf{x}_i^T)},$$

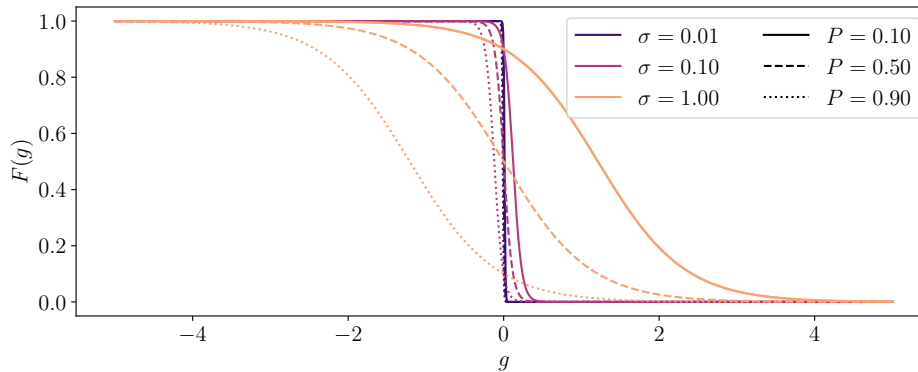


Fig. 1: SVGD particle systems with (b) and without (b) separating inducing and estimator particles.

An alternative to tracking  $q_T$  is to fit a Gaussian mixture (GM)  $\hat{q}_T$  to the final  $n$  samples following  $q_T$ . After resampling  $n$  samples from the GM  $\{\hat{\mathbf{x}}_i^T \sim \hat{q}_T\}_{i=1}^n$ , an SVRE-GM estimator can be constructed as

$$(3.7) \quad \hat{p}_{\mathcal{F}}^{\text{SVRE-GM}} = \frac{1}{n} \sum_{i=1}^n \hat{w}_i \quad \text{with} \quad \hat{w}_i := \mathbb{I}[g(\hat{\mathbf{x}}_i^T) \leq 0] \frac{p_0(\hat{\mathbf{x}}_i^T)}{\hat{q}_T(\hat{\mathbf{x}}_i^T)} \quad \text{and} \quad \hat{\delta}_{\mathcal{F}}^{\text{SVRE-GM}} = \sqrt{\frac{\sum_{i=1}^n \hat{w}_i^2}{(\sum_{i=1}^n \hat{w}_i)^2} - \frac{1}{n}}.$$

### 3.2 Algorithm and implementation details

**Sample split** Conceptually, the rare event setting presented in this work is somewhat different from the Bayesian inference applications tackled in the machine learning context, in which SVGD was conceived originally. In particular, evaluating the gradient of the log-likelihood or – in the context of rare events – the log-smooth indicator function, requires evaluating LSF gradients, which dominates computational cost in an engineering context. This is due to the fact that the computational model behind  $g$  is usually computationally expensive, e.g., a finite element or finite volume approximation of the solution to a set of partial differential equations. In the original SVGD, all  $n$  samples are used for two tasks simultaneously:

1. estimating the expectation in  $\phi_t$  in each step (see (2.12))
2. tracking the sequence of variational IS densities  $\{q_t\}_{t=1}^T$  (by propagation through  $\{\mathcal{T}_t\}_{t=1}^T$ )

It is, however, straight-forward to evaluate the empirical expectation using only a subset of all available samples and has first been proposed in [29]. This is useful as LSF gradients are required only for task 1. Once a set of samples for estimating the expectation is fixed, all samples are propagated through the  $\mathcal{T}_t$  (task 2), which only requires kernel evaluations and neither LSF nor LSF gradients. This bears a significant potential for reducing the overall number of required LSF gradient evaluations. In the context of importance sampling, performing task 1 on a subset of all samples has an additional advantage: the subset of all samples not used in task 1 remain independent and hence using only these samples in (3.5) renders the IS estimate unbiased [29, 45]. Assuming a total  $n + n_{\nabla}$  samples, we call the  $n_{\nabla}$  samples used for task 1 *inducing samples*, and the remaining  $n$  samples *estimation samples*. Fig. 2 shows a schematic illustrating this modification.

**Renormalization schemes** [38] suggest replacing the renormalization of the optimal map in (2.12) with an adagrad/RMSProp-like normalization term that accumulates gradient histories in an exponential moving average. That is, the learning rate in each step  $\epsilon_t$ , becomes a  $1 \times d$  vector of individual learning rates along each of the  $d$  dimensions and depends  $\mathbf{x}$ , i.e., is different for each particle. The transformation at step  $t$  then reads

$$(3.8) \quad \mathcal{T}_t(\mathbf{x}) = \mathbf{x} + \epsilon_t(\mathbf{x}) \odot \phi_t(\mathbf{x}) \quad (t = 1, \dots, T)$$

A more detailed description of RMSProp and the associated shape of  $\epsilon_t(\mathbf{x})$  is detailed in Appendix A. In the context of SVRE, we find this choice is effective for sampling from multimodal target IS densities, i.e.,

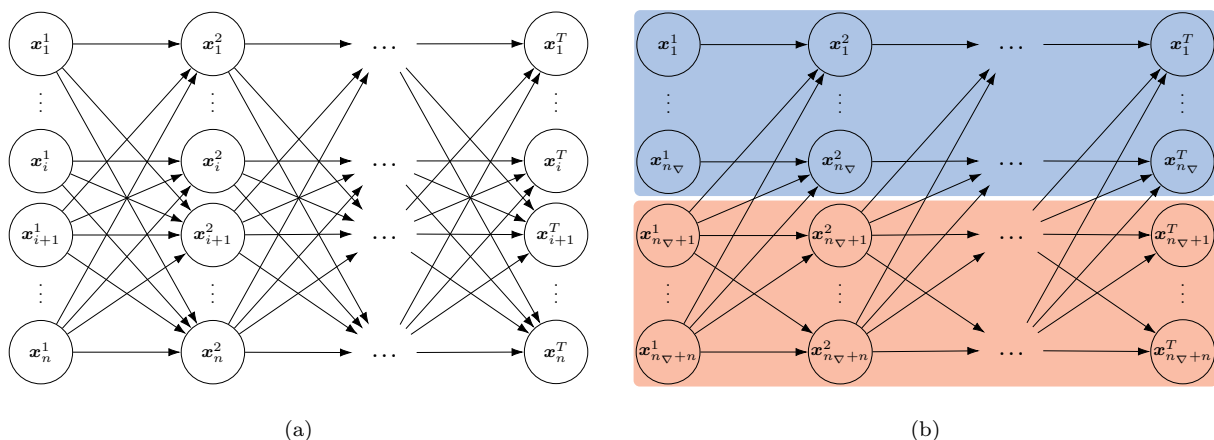


Fig. 2: SVGD particle systems without (a) and with (b) separating inducing and estimation samples (inspired by [29]). By convention, the first  $n_\nabla$  samples are used for constructing  $\mathcal{T}_t$  (blue box). The remaining  $n$  particles are propagated along  $\mathcal{T}_t$  and used for estimating  $p_{\mathcal{F}}$ .

when tackling problems with multiple relevant failure domains. For unimodal targets, renormalizing the optimal map to  $\ell_2$ -norm 1 in any step without any regard for gradient histories can outperform RMSProp. In particular for problems with a dominant variable and nearly axis-parallel streamlines (e.g. the plate example in [Subsection 4.3](#)), RMSProp tends to inflate the influence of less relevant variables and push samples in the wrong direction. In [Appendix A](#), we detail both renormalization schemes and how they affect the Jacobian  $\nabla_{\mathbf{x}}\mathcal{T}_t(\mathbf{x})$ . Unlike in [29], where the influence of  $\epsilon(\mathbf{x})$  in the Jacobian of the optimal map seems to be either ignored or approximated as constant with respect to  $\mathbf{x}$ , we account for said influence and derive the exact Jacobians under non-constant learning rates.

**Learning rate** A base learning rate  $\bar{\epsilon}_t$  is used to control the global step width independent of the renormalization scheme, i.e.  $\epsilon_t(\mathbf{x}) = \bar{\epsilon}_t/f(\mathbf{x})$ , where  $f(\cdot)$  represents the renormalization scheme (see [Appendix A](#)). In the original SVGD algorithm, the learning rate  $\bar{\epsilon}_t$  is chosen conservatively small, e.g.,  $\bar{\epsilon}_t = 0.001$ , which frequently leads to SVGD running for several hundred iterations until convergence. This in turn increases the overall number of required log-likelihood gradient evaluations. As discussed, in the rare event setting with an underlying expensive-to-evaluate computational model, model gradient evaluations dominate computational cost. Hence, our goal is to make  $\bar{\epsilon}_t$  as large as possible such that the total number of required LSF gradient evaluations becomes minimal, all while not inflating  $\bar{\epsilon}_t$  to the extent of compromising the invertibility of  $\mathcal{T}_t$ . In general, an  $\bar{\epsilon}_t$  striking a good balance between both desiderata will depend on the shape of  $g$ . Depending on the normalization scheme, our studies show values  $\bar{\epsilon}_t = 0.25 \dots 1.0$  are appropriate choices that lead to convergence in  $\mathcal{O}(-\log p_{\mathcal{F}})$  steps.

Alternatively, approximating the determinant of the Jacobian  $\nabla_{\mathbf{x}}\mathcal{T}_t(\mathbf{x})$  with a first-order approximation in  $\bar{\epsilon}_t$  both reduces the computational effort from  $\mathcal{O}(n^3)$  to  $\mathcal{O}(n)$  and renders the Jacobian determinant an explicit function of the base learning rate  $\bar{\epsilon}_t$ . Therefore, adopting the approximation, one can explicitly maximize  $\bar{\epsilon}$  in a corridor such that all Jacobian determinants (at all samples) are bounded away from zero and below an upper threshold in order to maximize convergence speed while guaranteeing computational stability. Details are provided in [Appendix B](#).

**Choice of kernel/bandwidth selection** In [38], the authors suggest using an isotropic Gaussian kernel

$$(3.9) \quad k(\mathbf{x}, \mathbf{y}) = \exp \left\{ -\frac{\|\mathbf{x} - \mathbf{y}\|^2}{2\ell^2} \right\}$$

with a single bandwidth parameter  $\ell$ . They suggest selecting  $\ell$  such that at any sample  $\mathbf{x}_i$ , the weights of all neighboring log-likelihood gradients balance with its own log-likelihood gradient, i.e.,  $\sum_{j \neq i} k(\mathbf{x}_i, \mathbf{y}_j) =$

$k(\mathbf{x}_i, \mathbf{y}_i) = 1$ . For an explicit choice of  $h$ , they approximate  $\sum_{i \neq j} k(\mathbf{x}_i, \mathbf{y}_j) \approx n \exp(-\text{median}(\|\mathbf{x} - \mathbf{y}\|)^2 / (2\ell^2))$  which yields  $\ell^2 = \text{median}(\|\mathbf{x} - \mathbf{y}\|)^2 / (2 \log n)$ . Our experiment suggest that – in combination with RMSProp renormalization – this is an advantageous choice for multimodal targets. For unimodal targets – for which we use  $\ell_2$ -normalization – setting  $\ell$  to a generic large value performs well (e.g.  $\ell = 10$  in standard normal space). The implication of this choice is that the effective gradient field will be an average of all  $\log p(\mathbf{x}_i)$  - values shared by all samples. Hence all samples move identically and the initial sample cloud moves towards the rare event region like a rigid body. In fact, if  $p_0$  belongs to exponential family and  $g$  is convex, it is easy to show that in the limit  $\ell \rightarrow \infty$  SVRE behaves like an exponential tilting IS estimate with the tilting parameter being the most probable point of the rare event (known as most probable point of failure or design point in reliability analysis).

Alternative choices of kernel are possible but have not been explored in this work. In particular, kernels with slowly decaying tails such as the inverse multiquadratic kernel have been found to offer theoretical advantages over kernels with exponentially decaying tails in Stein discrepancy-driven sampling methods [28].

### Algorithm

In this section we present a detailed pseudocode of the SVRE method and estimator in [Algorithm 2](#).

---

#### Algorithm 2: Stein variational rare event estimator (SVRE)

---

**Input** : LSF  $g(\mathbf{x})$ , smoother  $F(\mathbf{x})$  with  $\mu, \sigma$ , kernel  $k(\cdot, \cdot)$ , input PDF  $p_0, \delta_{\text{thresh}}, n, n_{\nabla}$

**Output**: failure estimate  $\hat{p}_{\mathcal{F}}$ , estimator c.o.v.  $\hat{\delta}_{\mathcal{F}}$ ,  $n$  independent  $q_T$ -samples

Initialize  $i = 1, \dots, n + \nabla n : \mathbf{x}_i^0 \sim p_0$  and  $\mathbf{q}_i^0 = p_0(\mathbf{x}_i^0)$

**while**  $\hat{\delta}_w > \delta_{\text{thresh}}$  **do**

    Propagate all particles ( $i = 1, \dots, n + n_{\nabla}$ ):

$$\mathbf{x}_i^{t+1} = \mathbf{x}_i^t + \epsilon_t \hat{\phi}_i^*(\mathbf{x}_i^t) \text{ with } \hat{\phi}_i^*(\mathbf{y}) = \frac{1}{n} \sum_{i=1}^{n_{\nabla}} k(\mathbf{x}_i^t, \mathbf{y}) [\nabla_{\mathbf{x}} \log F(\mathbf{x}_i^t) + \nabla_{\mathbf{x}} \log p_0(\mathbf{x}_i^t)] + \nabla_{\mathbf{x}} k(\mathbf{x}_i^t, \mathbf{y})$$

    Track the PDF of all independent particles ( $i = n_{\nabla} + 1, \dots, n_{\nabla} + n$ ):

$$q(\mathbf{x}_i^t) = q(\mathbf{x}_i^{t-1}) |\det \nabla \mathcal{T}_i(\mathbf{x}_i^{t-1})|^{-1}$$

**end**

SVRE: Estimate  $\hat{p}_{\mathcal{F}}^{\text{SVRE}}$  and  $\hat{\delta}_{\mathcal{F}}^{\text{SVRE}}$  according to (3.5) and (3.6)

SVRE-GM: Fit GM  $\hat{q}_T$  with  $\{\mathbf{x}_i^T\}_{i=1}^n$  and estimate  $\hat{p}_{\mathcal{F}}^{\text{SVRE-GM}}$  and  $\hat{\delta}_{\mathcal{F}}^{\text{SVRE-GM}}$  according to (3.7)

---

## 4 Numerical examples

**4.1 Error measures & algorithm settings** We quantify the accuracy of rare event probability estimates using the relative root-mean-squared error (relative RMSE):

$$(4.1) \quad \text{rRMSE} = \frac{1}{p_{\mathcal{F}}} \sqrt{\mathbb{E}[(p_{\mathcal{F}} - \hat{p}_{\mathcal{F}})^2]} = \frac{1}{p_{\mathcal{F}}} \sqrt{\underbrace{(p_{\mathcal{F}} - \mathbb{E}[\hat{p}_{\mathcal{F}}])^2}_{\text{bias}^2} + \underbrace{\mathbb{V}[\hat{p}_{\mathcal{F}}]}_{\text{variance}}} = \sqrt{\underbrace{\left(\frac{p_{\mathcal{F}} - \mathbb{E}[\hat{p}_{\mathcal{F}}]}{p_{\mathcal{F}}}\right)^2}_{\text{rel. bias}^2} + \underbrace{\frac{\mathbb{V}[\hat{p}_{\mathcal{F}}]}{p_{\mathcal{F}}^2}}_{\text{c.o.v.}^2}}.$$

Where reference results are available, we compare the relative RMSE produced by rare event-SVGD with state-of-the-art gradient-based rare event simulation methods such as HMC-based subset simulation [61] and importance sampling [48] (Approximate Sampling Target with Postprocessing Adjustment – ASTPA). In both these references as well as for SVRE, 500 independent randomly initialized runs of the method are used to estimate the expectation in (4.1). Unless noted otherwise, we run the SVRE algorithm with  $n_{\nabla} = 20$ ,  $\delta_{\text{thresh}} = 5$  and  $\bar{\epsilon} = 0.1 \dots 1$  depending on the choice of renormalization scheme for  $\epsilon_t$ .

In general, SVRE may be run with arbitrary absolutely continuous input distribution  $p_0$ . For the numerical experiments in this work, the input random vector  $\mathbf{X}$  is transformed to standard-normal space such that  $p_0$  is the standard-normal PDF. This facilitates a unified implementation of SVRE for arbitrary input distributions (given an isoprobabilistic transformation from  $\mathcal{X}$  to standard-normal space) and choosing non-adaptive kernel bandwidths in a problem-independent manner. We draw initial samples from the standard-normal  $p_0$  by transforming a low-discrepancy (Sobol') sequence [43].

With the exception of the random initial sample, SVRE – as SVGD – is a deterministic algorithm. It has been pointed out that such deterministic particle-based inference algorithms are more prone to *catastrophic convergence* than fully stochastic approaches such as MCMC or stochastic gradient descent methods [63, 15, 64]. In our experiments, this concerns a relatively small percentage of all 500 runs (less than 5% in any experiment). These cases can be identified reliably as they are associated with large estimator coefficients of variation. Therefore, we exclude these runs ( $\widehat{\delta}_{\mathcal{F}}^{\text{SVRE}} > 0.5$ ) from relative RMSE computations.

## 4.2 Test functions

**4.2.1 Linear LSF** The following linear limit-state function is a standard testbed example from reliability analysis and rare event simulation [47, 57] (see Fig. 3, left). It reads

$$g(\mathbf{x}) = \beta - \frac{1}{\sqrt{d}} \sum_{i=1}^d x_i, \quad \nabla g(\mathbf{x}) = -\frac{1}{\sqrt{d}} \mathbf{1}, \quad \mathbf{x} \sim \mathcal{N}(\mathbf{0}, \mathbf{I})$$

The exact rare event probability is available in closed form as  $p_{\mathcal{F}} = \Phi(-\beta)$  where  $\Phi(\cdot)$  is the cumulative distribution function of a standard-normal random variable. The reference solution is dimension-independent and the problem lends itself well to investigate the performance of rare event simulation algorithms in a simple setting across varying problem dimension with prescribed target probability level. Table 1 shows a

Table 1: Error (rRMSE) and cost (required number of model and model gradient evaluations) comparison of  $p_{\mathcal{F}}$ -estimates by HMC-SS [61], ASTPA [48] and our method for the linear LSF with  $d = 100$ . SVRE parameters are chosen as  $n_{\nabla} = 20$ ,  $cv_{\text{thresh}} = 5$ ,  $\bar{\epsilon} = 1$ .

LSF parameter (reference failure probability)		rRMSE			gradient (+ model) calls		
		[48]	[61]	SVRE	[48]	[61]	SVRE
<b>Linear</b>	$\beta = 4$ ( $p_{\mathcal{F}} = 3.17 \cdot 10^{-5}$ )	0.29	0.21	0.08	5617 (+0)	4600 (+0)	72 (+1000)
	$\beta = 5$ ( $p_{\mathcal{F}} = 2.87 \cdot 10^{-7}$ )	0.30	0.28	0.10	6641 (+0)	6400 (+0)	93 (+1000)
	$\beta = 6$ ( $p_{\mathcal{F}} = 0.99 \cdot 10^{-9}$ )	0.23	0.35	0.11	7635 (+0)	8731 (+0)	112 (+1000)
	$\beta = 7$ ( $p_{\mathcal{F}} = 1.28 \cdot 10^{-12}$ )	0.29	-	0.11	8639 (+0)	-	132 (+1000)

comparison of relative RMSE and total number of LSF and LSF gradient evaluations produced by two HMC-based reference methods and our SVRE algorithm at different target probability levels between  $\mathcal{O}(10^{-5})$  and  $\mathcal{O}(10^{-12})$  and for  $d = 100$ . The relative RMSE of HMC-based subset simulation [61] increases with decreasing target probability where as ASTPA [48] and SVRE errors are independent of the target probability magnitude. At around 10 %, the SVRE is noticeably smaller than that of the other two methods while generating a speedup of two orders of magnitude (in terms of LSF gradient evaluations).

**4.2.2 Quadratic LSF** Adding a quadratic term to the linear LSF from Subsection 4.2.1 in the  $x_1$ - $x_2$ -plane leads to the following quadratic LSF (see Fig. 3, center):

$$g(\mathbf{x}) = \beta + \frac{\kappa}{4}(x_1 - x_2)^2 - \frac{1}{\sqrt{d}} \sum_{i=1}^d x_i, \quad \nabla g(\mathbf{x}) = \left[ \frac{\kappa}{2}(x_1 - x_2) - 1/\sqrt{d}, -\frac{\kappa}{2}(x_1 - x_2) - 1/\sqrt{d}, -\frac{1}{\sqrt{d}} \mathbf{1} \right],$$

where  $\mathbf{x} \sim \mathcal{N}(\mathbf{0}, \mathbf{I})$ .  $\kappa$  governs the curvature of the LSF at the most probable point of failure and larger  $\kappa$  implies larger curvature, which in turn implies smaller  $p_{\mathcal{F}}$  [17]. Typical choices are  $\kappa = -1 \dots 10$  [61], where in this work we present results for the highest curvature setting at  $\kappa = 10$ . The exact failure probability corresponding to  $\kappa = 10$  can be computed analytically to  $p_{\mathcal{F}} = 4.73 \cdot 10^{-6}$ . Table 2 summarizes the computational cost and accuracy of SVRE as obtained from our numerical experiments as well as the performance of two gradient-based reference methods based on HMC. We compare three different settings of SVRE, among them two settings using RMSProp renormalization and either a constant base learning rate of  $\bar{\epsilon} = 0.1$  or an adaptive base learning rate as well as one setting using  $\ell_2$  renormalization. Reference results are available in the literature from ASTPA at  $d = 2$  and from HMC-SS at  $d = 100$ .

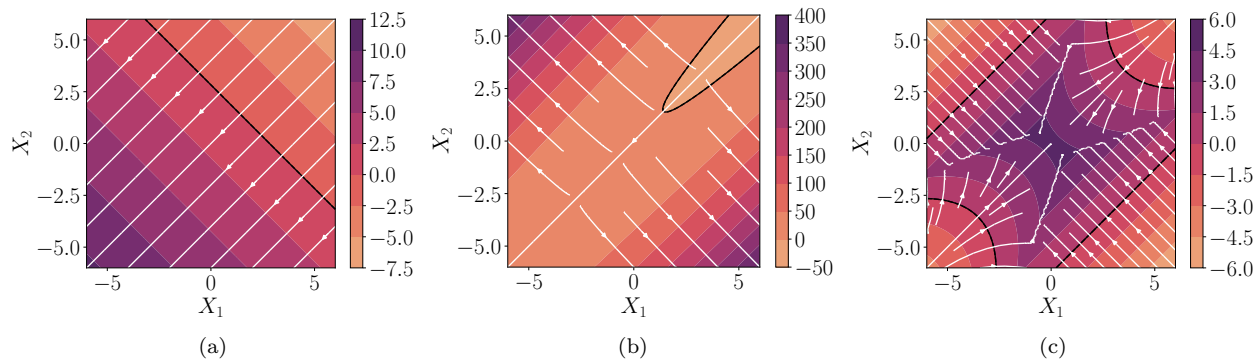


Fig. 3: Contour plots of the three considered test LSFs with failure hypersurface  $G(\mathbf{X}) = 0$  (black line) and streamlines of the LSFs (white lines). Left: linear LSF with  $d = 2$ , center: quadratic LSF with  $d = 2$ , right: four branch LSF.

Table 2: Error (rRMSE) and cost(required number of model and model gradient evaluations) comparison of  $p_{\mathcal{F}}$ -estimates by HMC-SS [61], ASTPA for rare events [48] and our method for the quadratic LSF. SVRE parameters are chosen as  $n_{\nabla} = 20$ ,  $cv_{\text{thresh}} = 5$ ,  $\bar{\epsilon} = 1$ .

dimension	rRMSE					gradient (+ model) calls					
	[48]	[61]	SVRE ( $\bar{\epsilon} = 0.1$ )	SVRE (adapt $\bar{\epsilon}$ )	SVRE ( $\ell_2$ )	[48]	[61]	SVRE ( $\bar{\epsilon} = 0.1$ )	SVRE (adapt $\bar{\epsilon}$ )	SVRE ( $\ell_2$ )	
<b>Quadratic</b>	$d = 2$	0.18	-	0.14	0.12	0.11	573 (+0)	-	443 (+10 <sup>3</sup> )	202 (+10 <sup>3</sup> )	356 (+10 <sup>3</sup> )
	$d = 100$	-	0.31	0.18	0.14	0.20	- (+0)	19747 (+10 <sup>3</sup> )	88 (+10 <sup>3</sup> )	86 (+10 <sup>3</sup> )	341 (+10 <sup>3</sup> )

The relative RMSE of all three SVRE versions is between 10 % and 20 % and consistently lower than the reference solutions in both dimensional settings. The required number of gradient evaluations is slightly lower compared to ASTPA in  $d = 2$  and significantly (by more than two orders of magnitude) lower than that of HMC-SS in  $d = 100$ . SVRE requires less steps to move samples to the rare event in the high-dimensional setting and hence, the total number of LSF gradients required is smaller in that setting. In the low-dimensional setting, however, gradient evaluations are reduced by more than half when the base learning rate  $base\epsilon$  is chosen adaptively according to Appendix A.

**4.2.3 Four branch LSF** The following four branch LSF is useful to test the SVRE performance on problems with several (here: four) relevant failure domains, (see Fig. 3, right):

$$g(\mathbf{x}) = \beta - \min \begin{cases} g_1 = 0.1(x_1 - x_2)^2 - (x_1 + x_2)/\sqrt{2} + 3 \\ g_2 = 0.1(x_1 - x_2)^2 + (x_1 + x_2)/\sqrt{2} + 3 \\ g_3 = x_1 - x_2 + 7/\sqrt{2} \\ g_4 = x_2 - x_1 + 7/\sqrt{2} \end{cases}, \nabla g(\mathbf{x}) = - \begin{cases} [0.2(x_1 - x_2) - 1/\sqrt{2}, -0.2(x_1 - x_2) - 1/\sqrt{2}], & \mathbf{x} \in g_1 \\ [0.2(x_1 - x_2) + 1/\sqrt{2}, -0.2(x_1 - x_2) + 1/\sqrt{2}], & \mathbf{x} \in g_2 \\ [1 + 7/\sqrt{2}, -1 + 7/\sqrt{2}], & \mathbf{x} \in g_3 \\ [-1 + 7/\sqrt{2}, 1 + 7/\sqrt{2}], & \mathbf{x} \in g_4 \end{cases}$$

where  $\mathbf{x} \sim \mathcal{N}(\mathbf{0}, \mathbf{I})$  and the target rare event probability depends on  $\beta$ . We investigate  $\beta = 0, 2, 4$ , which correspond to probabilities between  $4.45 \cdot 10^{-3}$  and  $5.57 \cdot 10^{-9}$ . Table 3 shows the performance of the SVRE estimator using 50 and 100 gradient samples per iteration as well as an SVRE-GM estimator using  $n_{\nabla} = 50$  and compares these to ASTPA results stated in [48] for the case  $\beta = 0$  (no reference results are available for larger  $\beta$ ). ASTPA performs on par with the SVRE estimators in terms of relative RMSE however requires slightly more gradient evaluations overall. SVRE-GM outperforms both SVRE and ASTPA

Table 3: Error (rRMSE) and cost (required number of model and model gradient evaluations) comparison of  $p_{\mathcal{F}}$ -estimates by HMC-SS [61], ASTPA [48] and our method for the four branch LSF. SVRE parameters are chosen as  $\delta_{\text{thresh}} = 5$ ,  $\bar{\epsilon} = 0.25$ .

	LSF parameter ( $p_{\mathcal{F}}$ )	rRMSE				gradient (+ model) calls			
		[48]	SVRE-GM	SVRE		[48]	SVRE-GM	SVRE	
			$n_{\nabla} = 50$	$n_{\nabla} = 50$	$n_{\nabla} = 100$		$n_{\nabla} = 50$	$n_{\nabla} = 50$	$n_{\nabla} = 100$
<b>Four Branch</b>	$\beta = 0$ ( $4.451 \cdot 10^{-3}$ )	0.18	0.14	0.24	0.21	573 (+0)	172.4 (+10 <sup>3</sup> )	197.3 (+10 <sup>3</sup> )	405.2 (+10 <sup>3</sup> )
	$\beta = 2$ ( $9.620 \cdot 10^{-6}$ )	-	0.21	0.33	0.31	-	314.1 (+10 <sup>3</sup> )	336.4 (+10 <sup>3</sup> )	750.8 (+10 <sup>3</sup> )
	$\beta = 4$ ( $5.596 \cdot 10^{-9}$ )	-	0.21	0.36	0.26	-	440.0 (+10 <sup>3</sup> )	548.9 (+10 <sup>3</sup> )	1746.4 (+10 <sup>3</sup> )

in the four branch example achieving lower relative RMSE with less gradient evaluations across all considered cases. Both SVRE/SVRE-GM errors as well as the total number of gradient evaluations increase moderately with decreasing target probability. The latter is expected as the total number of iterations to convergence scales approximately linearly with the magnitude of the target probability. Increasing  $n_{\nabla}$  from 50 to 100 consistently reduces the relative RMSE and average doubles the total effort approximately.

### 4.3 Engineering examples

#### 4.3.1 Darcy flow across porous aquifer

##### 4.3.1.1 Problem description

We consider the following 1-D boundary value problem on  $D = [0, 1]$

$$(4.2) \quad y \in D : \quad \frac{d}{dy} \left( \kappa(y, \omega) \frac{du(y, \omega)}{dy} \right) = -J(y), \quad \frac{du(y, \omega)}{dy} \Big|_{y=0} = -F(\omega), \quad u(1, \omega) = 1,$$

where  $u(y, \omega)$  describes the pressure head resulting from the stochastic diffusivity field  $\kappa$  as well as the given Dirichlet ( $y = 1$ ) and von Neumann ( $y = 0$ ) boundary conditions.  $F(\omega)$  represents a random flux boundary condition at the left boundary of  $D$  and is modelled as a Gaussian with mean  $\mu_F = 2$  and variance  $\sigma_F^2 = 0.5$ . The diffusivity  $\kappa$  is modelled as a log-normal random field (RF), which is generated by discretizing the underlying Gaussian RF  $\ln \kappa$  with mean  $\mu_{\ln \kappa} = 1$ , variance  $\sigma_{\ln \kappa}^2 = 0.3$  and correlation kernel  $k(y - y') = \exp\{-|y - y'|/\ell\}$  ( $\ell = 0.1$ ) using a Karhunen-Loève-expansion with  $d - 1$  terms:

$$(4.3) \quad \kappa(y) = \exp \left\{ \mu_{\ln \kappa} + \sigma_{\ln \kappa} \sum_{i=1}^{d-1} \sqrt{\lambda_i^{\kappa}} \varphi_i^{\kappa}(y) \xi_i \right\}.$$

$\{\lambda_i^{\kappa}, \varphi_i^{\kappa}(y)\}_{i=1}^{d-1}$  are the first  $d - 1$  eigenpairs of the correlation kernel where the eigenvalues are ordered in descending order and  $\boldsymbol{\xi}$  is a  $d - 1$  dimensional standard-normal random vector. The source term  $J$  is modelled as a mixture of four Gaussian plumes located equidstantly across  $D$ , i.e.,

$$(4.4) \quad J(y) = 0.8 \sum_{i=1}^4 \mathcal{N}(y | \mu_i = 0.2 \cdot i, \sigma_i = 0.05).$$

We are interested in the maximum pressure head exceeding a critical value  $p_{\text{thresh}} = 2.7$ , hence the LSF is defined as

$$(4.5) \quad g(\mathbf{X}) = p_{\text{thresh}} - \max(u(y, \mathbf{X})),$$

where  $\mathbf{X} := [F, \xi_1, \dots, \xi_{d-1}]$ . This example is taken from and discussed in greater detail in [55].

### 4.3.1.2 Results

Fig. 4 shows a comparison of accuracy and cost for SVRE estimates of the maximum pressure exceedance probability resulting from the LSF (4.5) for problem dimensions  $d = [5, 10, 20, 50, 100]$ . The target probability increases with increasing  $d$ , i.e., increasing number of KLE terms in (4.3), yet remains on the order  $\mathcal{O}(10^{-5})$  in all investigated cases [55]. The relative RMSE of all SVRE estimates decay approximately with rate  $n^{-1/2}$ ,

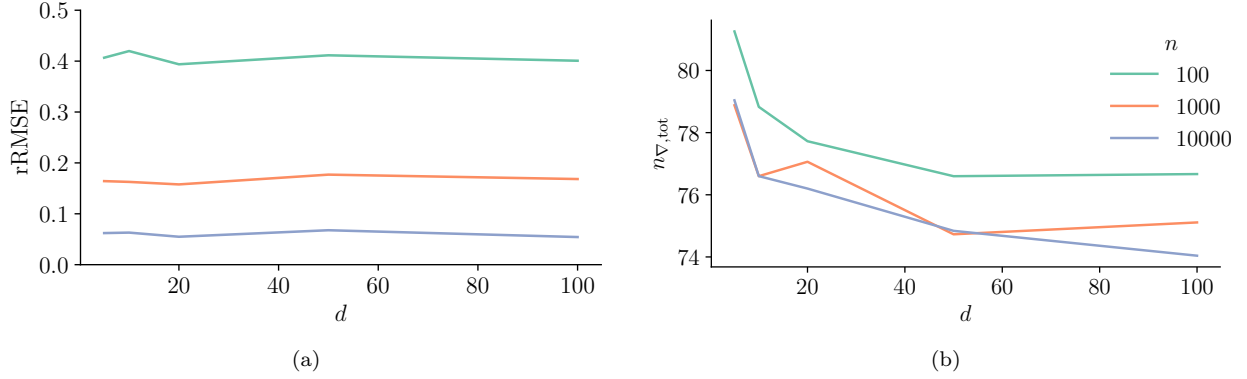


Fig. 4: Parameter study: SVRE accuracy (left) and cost (right) across different problem dimensions  $d$  while varying the number of samples used for estimating  $p_{\mathcal{F}}$ . SVRE parameters are chosen as  $n_{\nabla} = 20$ ,  $cv_{\text{thresh}} = 5$ ,  $\bar{\epsilon} = 1$ .

which is expected as the sample split described in Subsection 3.2 yields  $n$  independent samples for the IS estimate. Further, the error remains constant as  $d$  increases. The same is approximately true of the number of gradient evaluations required to build the estimates at different  $d$  and  $n$ . The total cost incurred of course still increases with  $n$  as it is equal to  $n_{\nabla, tot} + n$ . Fig. 4 shows SVRE accuracy and cost for varying parameters

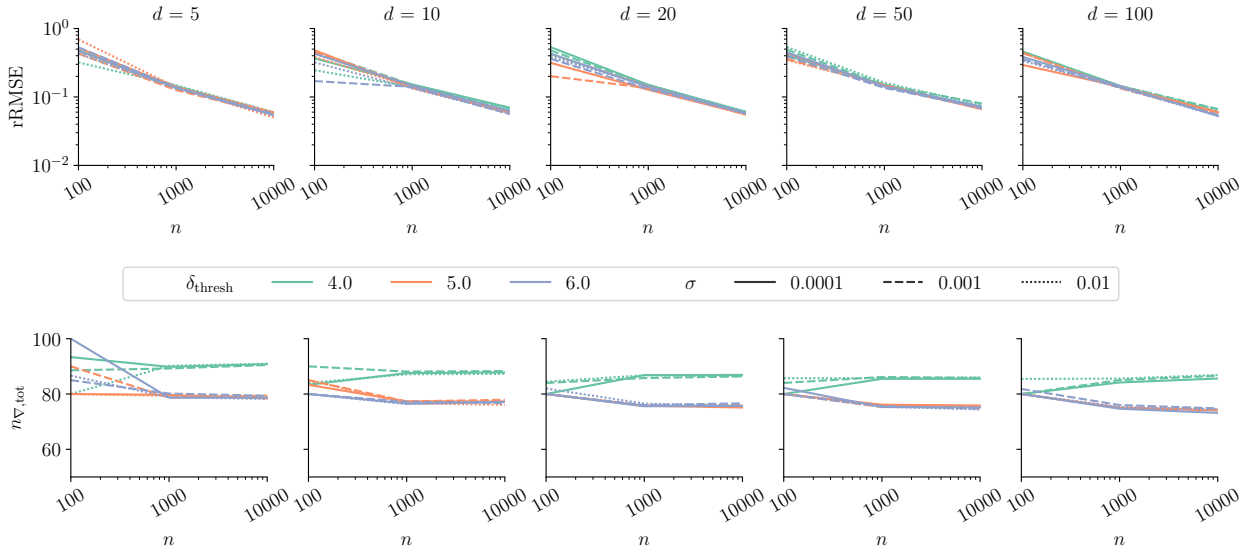


Fig. 5: Diffusion problem parameter study: relative RMSE (top) and cost in terms of total number of gradient evaluations per run (bottom) for various termination criteria  $\delta_{\text{thresh}}$  and degrees of smoothing  $\sigma$ .

$\sigma$  (the degree of LSF smoothing) and the exit criterion  $\delta_{\text{thresh}}$ . Both cost and accuracy of the SVRE estimator are insensitive to the choice of  $\sigma$  which is varied over two orders of magnitude ( $10^{-2} \dots 10^{-4}$ ). An intuitive finding is that choosing  $\delta_{\text{thresh}}$  smaller results in an increased overall number of gradient evaluations as the

method is run for more iterations on average. However, the estimator's accuracy also decreases if  $\delta_{\text{thresh}}$  is chosen too small, i.e., if the criterion for proximity of the IS distribution to the target distribution is too strict.

### 4.3.2 Steel plate in plane stress

#### 4.3.2.1 Problem description

We consider a modified version of the example given in [54, 35], which consists of a low-carbon steel plate of length 0.32 m, width 0.32 m, thickness  $t = 0.01$  m, and a hole of radius 0.02 m located at the center. The Poisson ratio is set to  $\nu = 0.29$  and the density of the plate is  $\rho = 7850$  kg/m<sup>3</sup>. The horizontal and vertical displacements are constrained at the left edge. The plate is subjected to a random surface load that acts on the right narrow plate side. The load is modelled as a log-normal random variable with mean  $\mu_q = 60$  MPa and  $\sigma_q = 12$  MPa. The plate's Young's modulus  $E(x, y)$  is considered uncertain and spatially

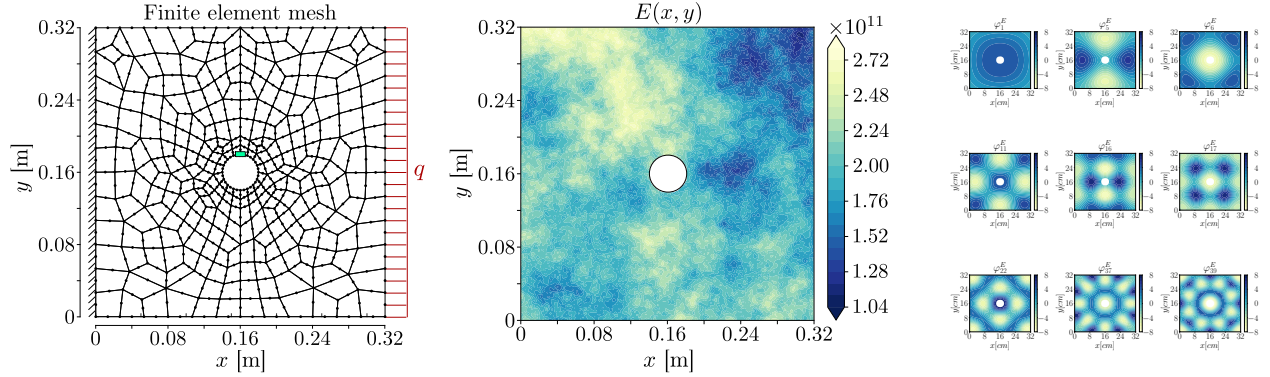


Fig. 6: Left: FE-mesh of 2D-plate model with control node of the first principal stress  $\sigma_1$ . Center: realization of the Young's modulus RF. Right: eigenfunctions of the isotropic exponential covariance kernel. Taken from [55] with permission.

variable. It is described by a homogeneous random field with lognormal marginal distribution, mean value  $\mu_E = 2 \times 10^5$  MPa and standard deviation  $\sigma_E = 3 \times 10^4$  MPa. The autocorrelation function of the underlying Gaussian field  $\ln E$  is modeled by the isotropic exponential model

$$(4.6) \quad \rho_{\ln E}(\Delta x, \Delta y) = \exp \left\{ -\frac{\sqrt{\Delta x^2 + \Delta y^2}}{l_E} \right\}$$

with correlation length  $l_{\ln E} = 0.04$ m. The Gaussian random field  $\ln E$  is discretized by a Karhunen-Loève-expansion with  $d_E = 868$ , which yields a mean error variance of 7.5% and reads

$$(4.7) \quad E(x, y) = \exp \left\{ \mu_{\ln E} + \sigma_{\ln E} \sum_{i=1}^{d_E} \sqrt{\lambda_i^E} \varphi_i^E(x, y) \xi_i \right\}.$$

$\mu_{\ln E}$  and  $\sigma_{\ln E}$  are the parameters of the log-normal marginal distribution of  $E$ ,  $\{\lambda_i^q, \varphi_i^q\}$  are the eigenpairs of the correlation kernel in (4.6) (see Fig. 6) and  $\boldsymbol{\xi} \in \mathbb{R}^{d \times 1}$  is a standard-normal random vector. The most influential eigenfunctions (based on a global output-oriented sensitivity analysis of the plate model performed in [22]) are shown in Fig. 6 on the right.

Assuming plane stress, the displacement field  $\mathbf{u}(x_1, x_2) = [u_1(x_1, x_2), u_2(x_1, x_2)]^T$  and the strain field  $\boldsymbol{\varepsilon} = 0.5[\nabla \mathbf{u} + (\nabla \mathbf{u})^T]$  can be computed implicitly based on elasticity theory through a set of elliptic partial differential equations (Cauchy-Navier equations) [31]:

$$(4.8) \quad \nabla \left[ \frac{\nu E(x_1, x_2)}{1 - \nu^2} \text{tr}(\boldsymbol{\varepsilon}) \mathbf{I} + G(x_1, x_2) \boldsymbol{\varepsilon} \right] + \mathbf{B} = 0.$$

$G(x_1, x_2) := E(x_1, x_2)/(2(1 + \nu))$  is the plate material’s shear modulus,  $E(x_1, x_2)$  is its Young’s modulus, and  $\mathbf{B} = [b(x_1), b(x_2)]^T$  is the vector of (gravitational) body forces acting on the plate. In order to solve (4.8), a finite element model with 282 eight-noded quadrilateral finite elements is used (Fig. 6).

The LSF is defined by means of a threshold for the the first principal plane stress

$$\sigma_1 = 0.5(\sigma_x + \sigma_y) + \sqrt{[0.5(\sigma_x + \sigma_y)]^2 + \tau_{xy}^2}$$

evaluated at node 11 (see green marker Fig. 6, left). Node 11 indicates a location where maximum plane stresses occur frequently in this example. The LSF reads

$$(4.9) \quad g(\mathbf{X}) = \sigma_{\text{threshold}} - \sigma_1(\mathbf{X}),$$

where  $\mathbf{X} := [q, \boldsymbol{\xi}]$  and  $\sigma_{\text{threshold}} = 196.133$  MPa. The target probability of failure is determined as  $p = 9.51 \cdot 10^{-7}$  with CoV = 0.0431 as the average of 100 repeated runs of subset simulation [5] with  $10^3$  samples per level.

#### 4.3.2.2 Results

Table 4 shows a comaprison of SVRE using  $n = 500$  and  $n = 5000$  estimation samples with iCEred [54] in terms of relative RMSE and the number of LSF and LSF gradient evaluations. iCEred is a subspace cross-entropy importance sampling method for rare event estimation that uses LSF gradients to inform the choice of subspace. We run SVRE with  $\ell_2$ -renormalization, base learning rate  $\bar{\epsilon} = 1$  and  $\delta_{\text{thresh}} = 5$ . In [54] a slightly larger probability of  $3.75 \cdot 10^{-6}$  is targeted. [54] report estimator coefficient of variation and mean calculated from 40 repeated runs, from which the relative RMSE is computed according to(4.1). With 6 %,

Table 4: Comparison or relative root mean squared error (rRMSE) and required number of model and model gradient evaluations of  $p_{\mathcal{F}}$ -estimates by CEBUred for rare events [54] and our method with  $n_{\nabla} = 20$ ,  $\delta_{\text{thresh}} = 5$ ,  $\bar{\epsilon} = 1$ .

example	dimension	rRMSE			gradient (+ model) calls		
		[54]	SVRE ( $n = 500$ )	SVRE ( $n = 5000$ )	[54]	SVRE ( $n = 500$ )	SVRE ( $n = 5000$ )
<b>Steel Plate</b>	$d = 869$ ( $p_{\mathcal{F}} = 9.51 \cdot 10^{-7}$ )	0.060	0.145	0.069	3037 (+3685)	103.64 (+500)	103.58 (+5000)

iCEred achieves the best relative RMSE, but using SVRE with 5000 estimation samples performs only slightly worse at 6.9% relative RMSE while using a mere 3% of the LSF gradient evaluations required for iCEred. In general, iCEred is tailored to high-dimensional problems with important low-dimensional subspaces and is therefore expected to achieve smaller errors in the plate problem. The total number of iCEred gradient samples could likely be reduced without increasing the relative RMSE by selecting  $n_{\nabla}$  adaptively in each step. This has been introduced in the context of reduced space cross-entropy importance sampling for Bayesian inference in [21].

Table 5: Comparison or relative root mean squared error (rRMSE) and required number of model and model gradient evaluations of  $p_{\mathcal{F}}$ -estimates by our method for different model dimensions with  $n_{\nabla} = 20$ ,  $\delta_{\text{thresh}} = 5$ ,  $\bar{\epsilon} = 1$ .

example	dimension (average $p_{\mathcal{F}}$ from 500 SVRE runs )	rRMSE	gradient (+ model) calls
<b>Steel Plate</b>	$d = 100$ ( $p_{\mathcal{F}} = 4.62 \cdot 10^{-7}$ )	0.101	91.44 (+ $10^3$ )
	$d = 500$ ( $p_{\mathcal{F}} = 7.92 \cdot 10^{-7}$ )	0.101	89.20 (+ $10^3$ )
	$d = 869$ ( $p_{\mathcal{F}} = 9.51 \cdot 10^{-7}$ )	0.113	103.16 (+ $10^3$ )

Table 5 shows SVRE results in different dimensions for the plate problem. As in the diffusion problem, different  $d$ -settings correspond to the number of terms in the KLE. With  $n = 1000$  estimation samples the relative RMSE is approximately constant around 10% in all dimensional settings. With the exception of a 10% increase between  $d = 500$  and  $d = 869$ , the same is true of the computational cost. The target probability decreases with decreasing dimension, which can be attributed to resolving less total variance of the Young’s modulus random field with less KLE terms [54].

**5 Conclusion** We have proposed a method termed Stein variational rare event simulation (SVRE) to sample from rare events and estimate the associated rare event probability. SVRE relies on Stein variational gradient descent (SVGD) – an approach for sampling from non-normalized distributions proposed in the context of Bayesian inference of probabilistic machine learning models [38]. We reformulate SVGD to move samples initially drawn from a tractable input distribution towards a near-optimal rare event importance sampling density. This is done by interpreting the indicator function of the rare event as a likelihood and smoothening it. Propagating samples repeatedly along streamlines of a specific set of velocity fields that are constructed in a reproducing kernel Hilbert space (RKHS) optimally reduces the KL divergence between the empirical distribution of the samples and the target distribution, i.e., the smoothened rare event IS distribution. Once the propagated samples have an empirical distribution sufficiently close to the target (in terms of Kullback-Leibler-divergence), they are used to construct an importance sampling estimate of the rare event probability.

We investigate two different methods for rescaling the optimal velocity field in each step and suggest an approximation for tracking velocity field determinants that allows to track the density of the particles. The approximation facilitates adaptively choosing the base learning rate that controls the convergence speed of the method. Further we suggest an exit criterion for when to stop evolving samples and building the importance sampling estimate.

We gauge the performance of SVRE against three state-of-the-art gradient-based rare event sampling algorithms. We examine performance and efficiency of the SVRE estimator using five numerical examples spanning problem dimensions between  $d = 2$  and  $d = 869$ . We find our SVRE estimator performs better or on par with several state-of-the-art rare event simulation methods while reducing the required number of model gradient evaluations by at least one and in some cases up to three orders of magnitude. This is relevant as gradient evaluations both are responsible for most of the computational effort associated with gradient-based rare event simulation algorithms as well as the facilitator for superior performance in complicated problems and for extremely small target probabilities ( $10^{-9} - 10^{-12}$ ) compared to gradient-free methods.

While we show that the SVRE estimator works well in several high-dimensional problems, the underlying SVGD method has been found to suffer from a variance degeneracy in high-dimensions [6]. Using distance-based kernels presents a second degeneracy that likely needs to be addressed to ensure SVRE works well in a very general high-dimensional setting [50]. An interesting direction for future research may thus be to flexibilize or generalize SVRE to work well in generic high dimensions, for example by investigating non-distance-based and heterotropic kernels. Alternatively, it is straight-forward to combine the SVRE with subspace approaches proposed in the context of SVGD such as [12, 39].

Given that the number of gradient evaluations is the computational bottleneck in the rare event setting, locally replacing  $g$  with a cheap gradient-true surrogate model may facilitate further efficiency gains. Such a surrogate model can be integrated in SVRE by considering a Stein operator with respect to the surrogate model and reweighting the RKHS by the likelihood ratio of the surrogate and the true target [30].

**6 Acknowledgment** This project was supported by the German Research Foundation (DFG) through grants STR 1140/11-1 and PA2901/1-1.

**Appendix A. Jacobian of the particle transformation at step  $t$ .** The particle transformation in the  $t$ -th step of SVGD reads

$$\begin{aligned}\mathcal{T}_t(\mathbf{x}) &= \mathbf{x} + \epsilon_t(\mathbf{x}) \odot \phi_t(\mathbf{x}) \\ \phi_t(\mathbf{x}) &= \sum_{i=1}^{n_\nabla} k(\mathbf{x}, \mathbf{y}_i) \nabla_{\mathbf{y}} \ln p(\mathbf{y}_i) + \nabla_{\mathbf{y}} k(\mathbf{x}, \mathbf{y}_i).\end{aligned}$$

This transformation has the form of a gradient descent with  $\phi_t(\mathbf{x})$  representing the objective gradient at  $\mathbf{x}$  and  $\epsilon_t$  is the step width or learning rate.  $\epsilon_t(\mathbf{x})$  may be adjusted along each coordinate of  $\mathcal{X}$  individually. In the stochastic gradient descent literature, it is common practice to rescale  $\epsilon_t(\mathbf{x})$  based on past and current gradient fields, hence it depends on  $\mathbf{x}$  through  $\phi_t$ . The Jacobian of  $\mathcal{T}_t(\mathbf{x})$  reads

$$\nabla_{\mathbf{x}} \mathcal{T}_t(\mathbf{x}) = \mathbf{I} + \text{diag } \epsilon_t(\mathbf{x}) \cdot \nabla_{\mathbf{x}} \phi_t(\mathbf{x}) + \text{diag } \phi_t(\mathbf{x}) \cdot \nabla_{\mathbf{x}} \epsilon_t(\mathbf{x}).$$

where

$$\nabla_{\mathbf{x}} \phi_t(\mathbf{x}) = \sum_{i=1}^{n_\nabla} \nabla_{\mathbf{x}} k(\mathbf{x}, \mathbf{y}_i) \nabla_{\mathbf{y}} \ln p(\mathbf{y}_i) + \nabla_{\mathbf{x}} \nabla_{\mathbf{y}} k(\mathbf{x}, \mathbf{y}_i).$$

In the original SVGD paper, the authors suggest using Adagrad [20] (or more precisely, a slightly improved version thereof called RMSProp) to select  $\epsilon_t$ . RMSProp rescales the current gradient field with an exponential moving average of past gradient fields, which reads

$$\begin{aligned}\epsilon_t(\mathbf{x}) &= \frac{\bar{\epsilon}_t}{\varepsilon + v_t(\mathbf{x})} \\ v_t^2(\mathbf{x}) &= \begin{cases} \phi_0^2, & t = 0 \\ \alpha^t \phi_0^2 + (1 - \alpha) \sum_{t'=1}^t \alpha^{t-t'} \phi_{t'}^2, & t > 0 \end{cases}.\end{aligned}$$

Therein,  $\phi_{t'}$  is the gradient field in step  $t' \leq t$  and  $\bar{\epsilon}_t$  is a base learning rate that acts equally on all coordinates and particles. The velocity of the moving average is controlled by  $\alpha$ , which is usually selected to be  $\alpha = 0.9$ .  $\varepsilon = 10^{-6}$  is a small nugget to avoid divide-by-zero errors.

Ignoring the nugget, the Jacobian of the RMSProp learning rate is  $\nabla_{\mathbf{x}} \epsilon_t(\mathbf{x}) \approx -\bar{\epsilon}_t \text{diag } v_t^{-2}(\mathbf{x}) \cdot \nabla_{\mathbf{x}} v_t(\mathbf{x})$ , where  $\mathbf{a}^b$  with  $\mathbf{a}$  a vector and  $b$  an integer denotes an elementwise power. We define

$$\phi_{\text{old}}^2 := \alpha^t \phi_0^2 + (1 - \alpha) \sum_{t'=1}^{t-1} \alpha^{t-t'} \phi_{t'}^2$$

and obtain

$$\nabla_{\mathbf{x}} v_t(\mathbf{x}) = \begin{cases} \nabla_{\mathbf{x}} \phi_t(\mathbf{x}), & t = 0 \\ (1 - \alpha) \text{diag}(\phi_t(\mathbf{x})/v_t(\mathbf{x})) \cdot \nabla_{\mathbf{x}} \phi_t(\mathbf{x}), & t > 0 \end{cases},$$

where  $\mathbf{a}/\mathbf{c}$  with  $\mathbf{a}$  and  $\mathbf{c}$  vectors is an elementwise division. Hence,

$$\nabla_{\mathbf{x}} \mathcal{T}_t(\mathbf{x}) \approx \mathbf{I} + \begin{cases} 0, & t = 0 \\ \bar{\epsilon}_t \text{diag}(\phi_{\text{old}}^2(\mathbf{x})/v_t^3(\mathbf{x})) \cdot \nabla_{\mathbf{x}} \phi_t(\mathbf{x}), & t > 0 \end{cases}$$

That is,  $\phi_{\text{old}}^2/v_t^3(\mathbf{x})$  adjusts the Jacobian of  $\mathcal{T}_t$  for the adaptive learning rate selection performed in RMSProp.

Instead of adjusting the learning rate differently along each dimension of  $\mathcal{X}$  as in RMSProp, we may want to preserve the original gradient field, so that  $\epsilon_t$  is a scalar depending on  $\mathbf{x}$ . In this case

$$\begin{aligned}\mathcal{T}_t(\mathbf{x}) &= \mathbf{x} + \epsilon_t(\mathbf{x}) \phi_t(\mathbf{x}) \\ \phi_t(\mathbf{x}) &= \sum_{i=1}^{n_\nabla} k(\mathbf{x}, \mathbf{y}_i) \nabla_{\mathbf{y}} \ln p(\mathbf{y}_i) + \nabla_{\mathbf{y}} k(\mathbf{x}, \mathbf{y}_i).\end{aligned}$$

The Jacobian of  $\mathcal{T}_t$  in this case reads

$$\nabla_{\mathbf{x}} \mathcal{T}_t(\mathbf{x}) = \mathbf{I} + \epsilon_t(\mathbf{x}) \cdot \nabla_{\mathbf{x}} \phi_t(\mathbf{x}) + \phi_t^T(\mathbf{x}) \cdot \nabla_{\mathbf{x}} \epsilon_t(\mathbf{x}).$$

An intuitive way to choose  $\epsilon_t$  is to renormalize each gradient evaluation, i.e., set  $\epsilon_t(\mathbf{x}) = \bar{\epsilon}_t \|\phi_t(\mathbf{x})\|^{-1}$ . With

$$\nabla_{\mathbf{x}} \|\phi_t(\mathbf{x})\|^{-1} = -\frac{\nabla_{\mathbf{x}} \|\phi_t(\mathbf{x})\|}{\|\phi_t(\mathbf{x})\|^2} = -\frac{\nabla_{\mathbf{x}} \phi_t(\mathbf{x}) \cdot \phi_t(\mathbf{x})}{\|\phi_t(\mathbf{x})\|^3}$$

we have

$$(A.1) \quad \nabla_{\mathbf{x}} \mathcal{T}_t(\mathbf{x}) \approx \mathbf{I} + \bar{\epsilon}_t \frac{\nabla_{\mathbf{x}} \phi_t(\mathbf{x})}{\|\phi_t(\mathbf{x})\|} \cdot \left( \mathbf{I} - \frac{\phi_t^T(\mathbf{x}) \cdot \phi_t(\mathbf{x})}{\|\phi_t(\mathbf{x})\|^2} \right).$$

**Appendix B. Trace approximation of  $\det(\nabla_{\mathbf{x}} \mathcal{T}_t)$ .** Evaluating log PDF of particles in generation  $t$ ,

$$\log q_t(\mathbf{x}) = \log q_0(\mathbf{x}) - \sum_{i=1}^t \log |\det(\nabla_{\mathbf{x}} \mathcal{T}_i(\mathbf{x}))|,$$

requires evaluating  $\det(\nabla_{\mathbf{x}} \mathcal{T}_t(\mathbf{x}))$  at all  $n$  particle locations, which costs  $\mathcal{O}(nd^3)$ . For small  $\bar{\epsilon}_t$ ,

$$\det \nabla_{\mathbf{x}} \mathcal{T}_t(\mathbf{x}) = \det(\mathbf{I} + \bar{\epsilon}_t \mathbf{A}) \approx 1 + \bar{\epsilon}_t \text{trace}(\mathbf{A}) \quad (+\mathcal{O}(\bar{\epsilon}_t^2))$$

is a useful approximation that reduces the overall cost from  $\mathcal{O}(nd^3)$  to  $\mathcal{O}(nd)$ . Therein,

$$A_{ij} = \epsilon_t(\mathbf{x}_i) \nabla_{x_j} \phi_t(\mathbf{x}_i) + \phi_t(\mathbf{x}_i) \nabla_{x_j} \epsilon_t(\mathbf{x}_i) \quad (\ell_2) \quad \text{or} \quad A_{ij} = \alpha \frac{\nabla_{x_j} \phi_t(\mathbf{x}) \phi_{\text{old},ij}^2}{v_{t,ij}^3(\mathbf{x})} \quad (\text{RMSPProp}).$$

Further, the approximation facilitates explicitly choosing  $\bar{\epsilon}_t$  such that  $\det(\nabla_{\mathbf{x}} \mathcal{T}_t(\mathbf{x}))$  is bounded at all particle locations and hence  $\mathcal{T}_t(\mathbf{x})$  is locally invertible at all particle locations.

## REFERENCES

- [1] R. J. ALLEN, D. FRENKEL, AND P. R. TEN WOLDE, *Simulating rare events in equilibrium or nonequilibrium stochastic systems.*, J Chem Phys, 124 (2006), p. 024102, <https://doi.org/10.1063/1.2140273>.
- [2] N. ARONSZAJN, *Theory of reproducing kernels*, Transactions of the American Mathematical Society, 68 (1950), pp. 337–404.
- [3] S. ASMUSSEN AND D. P. KROESE, *Improved algorithms for rare event simulation with heavy tails*, Advances in Applied Probability, 38 (2006), pp. 545–558.
- [4] S. AU AND J. BECK, *A new adaptive importance sampling scheme for reliability calculations*, Structural Safety, 21 (1999), pp. 135 – 158.
- [5] S.-K. AU AND J. L. BECK, *Estimation of small failure probabilities in high dimensions by subset simulation*, Probabilistic Engineering Mechanics, 16 (2001), pp. 263–277, [https://doi.org/https://doi.org/10.1016/S0266-8920\(01\)00019-4](https://doi.org/https://doi.org/10.1016/S0266-8920(01)00019-4), <https://www.sciencedirect.com/science/article/pii/S0266892001000194>.
- [6] J. BA, M. A. ERDOGDU, M. GHASSEMI, S. SUN, T. SUZUKI, D. WU, AND T. ZHANG, *Understanding the variance collapse of SVGD in high dimensions*, in International Conference on Learning Representations, 2022, <https://openreview.net/forum?id=Qycd9j5Qp9J>.
- [7] P. BEAUREPAIRE, H. JENSEN, G. SCHUËLLER, AND M. VALDEBENITO, *Reliability-based optimization using bridge importance sampling*, Probabilistic Engineering Mechanics, 34 (2013), pp. 48–57.
- [8] D. M. BLEI, A. KUCUKELBIR, AND J. D. MCAULIFFE, *Variational inference: A review for statisticians*, Journal of the American Statistical Association, 112 (2017), pp. 859–877, <https://doi.org/10.1080/01621459.2017.1285773>.
- [9] K. BREITUNG, *Asymptotic approximations for multinormal integrals*, Journal of Engineering Mechanics, 110 (1984), pp. 357–366.
- [10] C. G. BUCHER, *Adaptive sampling — an iterative fast Monte Carlo procedure*, Structural Safety, 5 (1988), pp. 119 – 126.
- [11] F. CÉROU, P. DEL MORAL, T. FURON, AND A. GUYADER, *Sequential monte carlo for rare event estimation*, Statistics and Computing, 22 (2012), pp. 795–808, <https://doi.org/10.1007/s11222-011-9231-6>.
- [12] P. CHEN AND O. GHATTAS, *Projected stein variational gradient descent*, in Advances in Neural Information Processing Systems, H. Larochelle, M. Ranzato, R. Hadsell, M. Balcan, and H. Lin, eds., vol. 33, Curran Associates, Inc., 2020, pp. 1947–1958.
- [13] M. CHIRON, C. GENEST, J. MORIO, AND S. DUBREUIL, *Failure probability estimation through high-dimensional elliptical distribution modeling with multiple importance sampling*, Reliability Engineering & System Safety, 235 (2023), p. 109238, <https://doi.org/https://doi.org/10.1016/j.ress.2023.109238>.

- [14] K. CHWIAKOWSKI, H. STRATHMANN, AND A. GRETTON, *A kernel test of goodness of fit*, in Proceedings of The 33rd International Conference on Machine Learning, M. F. Balcan and K. Q. Weinberger, eds., vol. 48 of Proceedings of Machine Learning Research, New York, New York, USA, 20–22 Jun 2016, PMLR, pp. 2606–2615.
- [15] F. D’ANGELO AND V. FORTUIN, *Annealed stein variational gradient descent*, 2021, <https://arxiv.org/abs/2101.09815>.
- [16] A. DER KIUREGHIAN, *First-and second-order reliability methods*, in Engineering Design Reliability Handbook, E. Nikolaidis, D. M. Ghiocel, and S. Singhal, eds., CRC Press, Boca Raton, FL, 2005, ch. 14.
- [17] O. DITLEVSEN AND H. O. MADSEN, *Structural reliability methods*, John Wiley & Sons Ltd, 1996.
- [18] A. DOUCET, N. DE FREITAS, AND N. J. GORDON, eds., *Sequential Monte Carlo Methods in Practice*, Statistics for Engineering and Information Science, Springer, 2001, <https://doi.org/10.1007/978-1-4757-3437-9>.
- [19] S. DUANE, A. KENNEDY, B. J. PENDLETON, AND D. ROWETH, *Hybrid monte carlo*, Physics Letters B, 195 (1987), pp. 216–222, [https://doi.org/https://doi.org/10.1016/0370-2693\(87\)91197-X](https://doi.org/https://doi.org/10.1016/0370-2693(87)91197-X).
- [20] J. DUCHI, E. HAZAN, AND Y. SINGER, *Adaptive subgradient methods for online learning and stochastic optimization*, Journal of Machine Learning Research, 12 (2011), pp. 2121–2159.
- [21] M. EHRE, R. FLOCK, M. FUSSEDER, I. PAPAIOANNOU, AND D. STRAUB, *Certified dimension reduction for bayesian updating with the cross-entropy method*, SIAM/ASA Journal on Uncertainty Quantification, 11 (2023), pp. 358–388, <https://doi.org/10.1137/22M1484031>.
- [22] M. EHRE, I. PAPAIOANNOU, AND D. STRAUB, *Global sensitivity analysis in high dimensions with PLS-PCE*, Reliability Engineering & System Safety, 198 (2020), p. 106861, <https://doi.org/https://doi.org/10.1016/j.res.2020.106861>, <http://www.sciencedirect.com/science/article/pii/S0951832019314140>.
- [23] P. EMBRECHTS, C. KLÜPPELBERG, AND T. MIKOSCH, *Modelling extremal events: for insurance and finance*, vol. 33, Springer Science & Business Media, 2013.
- [24] S. ENGELUND AND R. RACKWITZ, *A benchmark study on importance sampling techniques in structural reliability*, Structural Safety, 12 (1993), pp. 255 – 276.
- [25] M. FABER, *Statistics and Probability Theory: In Pursuit of Engineering Decision Support*, Topics in Safety, Risk, Reliability and Quality, Springer Netherlands, 2012, <https://books.google.de/books?id=HJAQYtyJwIsC>.
- [26] P. GLASSERMAN, P. HEIDELBERGER, P. SHAHABUDDIN, AND T. ZAJIC, *Multilevel splitting for estimating rare event probabilities*, Operations Research, 47 (1999), pp. 585–600, <https://doi.org/10.1287/opre.47.4.585>.
- [27] J. GORHAM AND L. MACKEY, *Measuring sample quality with stein’s method*, in Advances in Neural Information Processing Systems, C. Cortes, N. Lawrence, D. Lee, M. Sugiyama, and R. Garnett, eds., vol. 28, Curran Associates, Inc., 2015.
- [28] J. GORHAM AND L. MACKEY, *Measuring sample quality with kernels*, in Proceedings of the 34th International Conference on Machine Learning, D. Precup and Y. W. Teh, eds., vol. 70 of Proceedings of Machine Learning Research, PMLR, 06–11 Aug 2017, pp. 1292–1301.
- [29] J. HAN AND Q. LIU, *Stein variational adaptive importance sampling*, in Proceedings of the Thirty-Third Conference on Uncertainty in Artificial Intelligence, UAI 2017, Sydney, Australia, August 11-15, 2017, G. Elidan, K. Kersting, and A. T. Ihler, eds., AUAI Press, 2017, <http://auai.org/uai2017/proceedings/papers/217.pdf>.
- [30] J. HAN AND Q. LIU, *Stein variational gradient descent without gradient*, 2018, <https://doi.org/10.48550/ARXIV.1806.02775>, <https://arxiv.org/abs/1806.02775>.
- [31] C. JOHNSON, *Numerical solution of partial differential equations by the finite element method*, Dover Publications, 2009.
- [32] A. KORBA, A. SALIM, M. ARBEL, G. LUISE, AND A. GRETTON, *A non-asymptotic analysis for stein variational gradient descent*, in Advances in Neural Information Processing Systems, H. Larochelle, M. Ranzato, R. Hadsell, M. Balcan, and H. Lin, eds., vol. 33, Curran Associates, Inc., 2020, pp. 4672–4682.
- [33] M. LEMAIRE, A. CHATEAUNEUF, AND J.-C. MITTEAU, *Structural reliability*, Wiley-ISTE, 2009.
- [34] C. LIU, J. ZHUO, P. CHENG, R. ZHANG, AND J. ZHU, *Understanding and accelerating particle-based variational inference*, in Proceedings of the 36th International Conference on Machine Learning, K. Chaudhuri and R. Salakhutdinov, eds., vol. 97 of Proceedings of Machine Learning Research, PMLR, 09–15 Jun 2019, pp. 4082–4092.
- [35] P.-L. LIU AND K.-G. LIU, *Selection of random field mesh in finite element reliability analysis*, Journal of Engineering Mechanics, 119 (1993), pp. 667–680.
- [36] Q. LIU, *Stein variational gradient descent as gradient flow*, in Advances in Neural Information Processing Systems, I. Guyon, U. V. Luxburg, S. Bengio, H. Wallach, R. Fergus, S. Vishwanathan, and R. Garnett, eds., vol. 30, Curran Associates, Inc., 2017, [https://proceedings.neurips.cc/paper\\_files/paper/2017/file/17ed8abedc255908be746d245e50263a-Paper.pdf](https://proceedings.neurips.cc/paper_files/paper/2017/file/17ed8abedc255908be746d245e50263a-Paper.pdf).
- [37] Q. LIU, J. D. LEE, AND M. JORDAN, *A kernelized stein discrepancy for goodness-of-fit tests*, in Proceedings of the 33rd International Conference on International Conference on Machine Learning - Volume 48, ICML’16, JMLR.org, 2016, p. 276–284.
- [38] Q. LIU AND D. WANG, *Stein variational gradient descent: A general purpose bayesian inference algorithm*, in Advances in Neural Information Processing Systems, D. Lee, M. Sugiyama, U. Luxburg, I. Guyon, and R. Garnett, eds., vol. 29, Curran Associates, Inc., 2016, <https://proceedings.neurips.cc/paper/2016/file/b3ba8f1bee1238a2f37603d90b58898d-Paper.pdf>.
- [39] X. LIU, H. ZHU, J.-F. TON, G. WYNNE, AND A. DUNCAN, *Grassmann stein variational gradient descent*, in Proceedings of The 25th International Conference on Artificial Intelligence and Statistics, G. Camps-Valls, F. J. R. Ruiz, and I. Valera, eds., vol. 151 of Proceedings of Machine Learning Research, PMLR, 28–30 Mar 2022, pp. 2002–2021.
- [40] J. LU, Y. LU, AND J. NOLEN, *Scaling limit of the stein variational gradient descent: The mean field regime*, SIAM Journal on Mathematical Analysis, 51 (2019), pp. 648–671, <https://doi.org/10.1137/18M1187611>.
- [41] P. D. MORAL, A. DOUCET, AND A. JASRA, *Sequential monte carlo samplers*, Journal of the Royal Statistical Society. Series B (Statistical Methodology), 68 (2006), pp. 411–436.
- [42] R. M. NEAL, *MCMC using Hamiltonian dynamics*, Handbook of Markov Chain Monte Carlo, 54 (2010), pp. 113–162.
- [43] H. NIEDERREITER, *Random Number Generation and Quasi-Monte Carlo Methods*, Society for Industrial and Applied Mathematics, 1992, <https://doi.org/10.1137/1.9781611970081>, <https://epubs.siam.org/doi/abs/10.1137/1.9781611970081>.

- [44] N. NÜSKEN AND D. R. M. RENGER, *Stein variational gradient descent: Many-particle and long-time asymptotics*, Foundations of Data Science, (2023), pp. 0–0, <https://doi.org/10.3934/fods.2022023>, [/article/id/63b40317aa1db67769a1644a](https://doi.org/10.3934/fods.2022023/article/id/63b40317aa1db67769a1644a).
- [45] A. B. OWEN, *Monte Carlo theory, methods and examples*, 2013.
- [46] I. PAPAIOANNOU, W. BETZ, K. ZWIRGLMAIER, AND D. STRAUB, *Mcmc algorithms for subset simulation*, Probabilistic Engineering Mechanics, 41 (2015), pp. 89–103, <https://doi.org/https://doi.org/10.1016/j.probengmech.2015.06.006>.
- [47] I. PAPAIOANNOU, C. PAPADIMITRIOU, AND D. STRAUB, *Sequential importance sampling for structural reliability analysis*, Structural Safety, 62 (2016), pp. 66 – 75, <https://doi.org/http://dx.doi.org/10.1016/j.strusafe.2016.06.002>, <http://www.sciencedirect.com/science/article/pii/S0167473016300169>.
- [48] K. G. PAKONSTANTINOOU AND H. NIKBAKHT, *Hamiltonian mcmc methods for estimating rare events probabilities in high-dimensional problems*, 2020, <https://arxiv.org/abs/2007.00180>.
- [49] R. RACKWITZ AND B. FIESSLER, *Structural reliability under combined random load sequences*, Computers & Structures, 9 (1978), pp. 489 – 494, [https://doi.org/http://dx.doi.org/10.1016/0045-7949\(78\)90046-9](https://doi.org/http://dx.doi.org/10.1016/0045-7949(78)90046-9), <http://www.sciencedirect.com/science/article/pii/0045794978900469>.
- [50] J. R. S. P. B. S. A. . W. L. RAMDAS, A., *On the decreasing power of kernel and distance based nonparametric hypothesis tests in high dimensions*, in Proceedings of the AAAI Conference on Artificial Intelligence, vol. 29, 2015, <https://doi.org/https://doi.org/10.1609/aaai.v29i1.9692>.
- [51] G. RUBINO AND B. TUFFIN, *Rare Event Simulation using Monte Carlo Methods*, John Wiley & Sons, Ltd, 2009.
- [52] R. Y. RUBINSTEIN AND D. P. KROESE, *Simulation and the Monte Carlo Method*, Wiley Publishing, 3rd ed., 2017.
- [53] I. STEINWART AND A. CHRISTMANN, *Support Vector Machines*, Information Science and Statistics, Springer New York, 2008.
- [54] F. URIBE, I. PAPAIOANNOU, Y. M. MARZOUK, AND D. STRAUB, *Cross-entropy-based importance sampling with failure-informed dimension reduction for rare event simulation*, SIAM/ASA Journal on Uncertainty Quantification, 9 (2021), pp. 818–847, <https://doi.org/10.1137/20M1344585>.
- [55] F. URIBE-CASTILLO, *Bayesian analysis and rare event simulation of random fields*, PhD thesis, Technische Universität München, 2020.
- [56] M. VALDEBENITO, H. PRADLWARTER, AND G. SCHUËLLER, *The role of the design point for calculating failure probabilities in view of dimensionality and structural nonlinearities*, Structural Safety, 32 (2010), pp. 101 – 111, <https://doi.org/http://dx.doi.org/10.1016/j.strusafe.2009.08.004>, <http://www.sciencedirect.com/science/article/pii/S0167473009000617>.
- [57] F. WAGNER, J. LATZ, I. PAPAIOANNOU, AND E. ULLMANN, *Multilevel sequential importance sampling for rare event estimation*, SIAM Journal on Scientific Computing, 42 (2020), pp. A2062–A2087, <https://doi.org/10.1137/19M1289601>.
- [58] F. WAGNER, I. PAPAIOANNOU, AND E. ULLMANN, *The ensemble kalman filter for rare event estimation*, SIAM/ASA Journal on Uncertainty Quantification, 10 (2022), pp. 317–349, <https://doi.org/10.1137/21M1404119>.
- [59] D. WANG AND Q. LIU, *Learning to draw samples: With application to amortized MLE for generative adversarial learning*, CoRR, abs/1611.01722 (2016), <http://arxiv.org/abs/1611.01722>, <https://arxiv.org/abs/1611.01722>.
- [60] D. WANG AND Q. LIU, *Nonlinear stein variational gradient descent for learning diversified mixture models*, in Proceedings of the 36th International Conference on Machine Learning, K. Chaudhuri and R. Salakhutdinov, eds., vol. 97 of Proceedings of Machine Learning Research, PMLR, 09–15 Jun 2019, pp. 6576–6585.
- [61] Z. WANG, M. BROCCARDO, AND J. SONG, *Hamiltonian monte carlo methods for subset simulation in reliability analysis*, Structural Safety, 76 (2019), pp. 51–67, <https://doi.org/https://doi.org/10.1016/j.strusafe.2018.05.005>.
- [62] Z. WANG AND J. SONG, *Cross-entropy-based adaptive importance sampling using von Mises-Fisher mixture for high dimensional reliability analysis*, Structural Safety, 59 (2016), pp. 42–52.
- [63] M. WELLING AND Y. W. TEH, *Bayesian learning via stochastic gradient langevin dynamics*, in Proceedings of the 28th International Conference on Machine Learning, ICML 2011, Bellevue, Washington, USA, June 28 - July 2, 2011, L. Getoor and T. Scheffer, eds., Omnipress, 2011, pp. 681–688, [https://icml.cc/2011/papers/398\\_icmlpaper.pdf](https://icml.cc/2011/papers/398_icmlpaper.pdf).
- [64] J. ZHANG, R. ZHANG, L. CARIN, AND C. CHEN, *Stochastic particle-optimization sampling and the non-asymptotic convergence theory*, in Proceedings of the Twenty Third International Conference on Artificial Intelligence and Statistics, S. Chiappa and R. Calandra, eds., vol. 108 of Proceedings of Machine Learning Research, PMLR, 26–28 Aug 2020, pp. 1877–1887.
- [65] Y. ZHU AND N. ZABARAS, *Bayesian deep convolutional encoder–decoder networks for surrogate modeling and uncertainty quantification*, Journal of Computational Physics, 366 (2018), pp. 415–447, <https://doi.org/https://doi.org/10.1016/j.jcp.2018.04.018>.